AUTOIMMUNITY

Brain-resident memory T cells generated early in life predispose to autoimmune disease in mice

Karin Steinbach[1], Ilena Vincenti[1], Kristof Egervari[1,2], Mario Kreutzfeldt[1,2], Franziska van der Meer[3], Nicolas Page[1], Bogna Klimek[1], Irène Rossitto-Borlat[1], Giovanni Di Liberto[1], Andreas Muschaweckh[4], Ingrid Wagner[1], Karim Hammad[1], Christine Stadelmann[3], Thomas Korn[4,5], Oliver Hartley[1,6], Daniel D. Pinschewer[7], Doron Merkler[1,2]*

Epidemiological studies associate viral infections during childhood with the risk of developing autoimmune disease during adulthood. However, the mechanistic link between these events remains elusive. We report that transient viral infection of the brain in early life, but not at a later age, precipitates brain autoimmune disease elicited by adoptive transfer of myelin-specific $CD4^+$ T cells at sites of previous infection in adult mice. Early-life infection of mouse brains imprinted a chronic inflammatory signature that consisted of brain-resident memory T cells expressing the chemokine (C-C motif) ligand 5 (CCL5). Blockade of CCL5 signaling via C-C chemokine receptor type 5 prevented the formation of brain lesions in a mouse model of autoimmune disease. In mouse and human brain, $CCL5^+$ T_{RM} were located predominantly to sites of microglial activation. This study uncovers how transient brain viral infections in a critical window in life might leave persisting chemotactic cues and create a long-lived permissive environment for autoimmunity.

INTRODUCTION

Studies of discordant monozygotic twins strongly suggest that, besides genetic predisposition, environmental factors determine the risk of developing autoimmune disease, especially in multiple sclerosis (MS) (*1*). Most prominently, a history of virus infection is considered a key environmental contributor that increases the risk for development of autoimmune disease (*2*, *3*). Population migration studies imply that in areas of high MS prevalence, an increased environmental risk to develop MS is acquired before the age of 15 (*4*). Thus, a considerable amount of time may pass between the initial exposure to the environmental factor (such as viral infection) and first clinical manifestation of MS. To explain how virus infections can break self-tolerance mechanisms, several mutually nonexclusive concepts including molecular mimicry (*5*), epitope spreading (*6*), bystander activation (*7*), and viral déjà vu (*8*) have emerged from experimental model systems. Molecular mimicry and viral déjà vu are based on the presence of T cells that display cross-reactivity between a central nervous system (CNS) antigen with an encountered pathogen. Epitope spreading and bystander activation are mechanisms by which the inflammatory environment produced by an infection can enable the accidental priming of an autoreactive T cell response (*5*). It has been postulated that such pathogen-induced inflammatory changes in the tissue microenvironment may create a long-lived "fertile field," capable of fostering future autoimmune attacks (*9*). However, it remains unknown whether and how a transient virus infection of the brain could sustainably alter its microenvironment and thereby predispose the organ to the development of autoimmune disease.

Viral infections of the CNS can occasionally be lethal (*10*) but mostly cause only mild and transient febrile illness (*11*) and can even be cleared by the immune system without any apparent symptoms (*12*). However, such transient infections of the brain generate long-lived $CD69^+$ memory $CD8^+$ T cells that persist at sites of previous infection (*13*, *14*). These so-called resident memory T cells (T_{RM}) provide a powerful local defense system against reinfection in the brain (*13*), as well as in other nonlymphoid tissues (*15*–*19*). Reactivation of T_{RM} by a recurrent infection triggers activation and recruitment of multiple leukocyte subsets into the tissue (*19*, *20*). In humans, brain T_{RM} (bT_{RM}) have been found in healthy and diseased human brains (*21*, *22*); however, it remains unknown whether T_{RM} could also be potentially involved in the establishment of durable local fertile fields for subsequent autoimmune attack.

Lymphocytic choriomenigitis virus (LCMV) is a natural pathogen of the mouse that can occasionally be transmitted to humans (*23*). Several wild-type (WT) and reverse-engineered mutant strains of LCMV have proven to be valuable tools for studying antiviral immunity and host-pathogen interactions in a variety of experimental settings, including transient and persisting infection (*13*, *24*–*28*). Intracranial infection with an attenuated strain of LCMV-expressing vesicular stomatitis virus Indiana glycoprotein [rLCMV/INDG (*29*), hereafter referred to as rLCMV] is an established model to study transient brain infection in adult immunocompetent C57BL/6 mice (*13*, *28*).

Here, we used this model to investigate whether transient infections in early life (EL) predispose to autoimmune diseases of the brain later in life. We found that transient brain infection in EL generates a persisting and long-lived proinflammatory microenvironment at sites of previous infection that fosters the precipitation of autoimmune lesions. Chemokine (C-C motif) ligand 5 (CCL5)–producing bT_{RM}, which clustered at sites of previous virus infection together with major histocompatibility complex II (MHCII)–positive myeloid cells, are a critical component of this autoimmune lesion-prone microenvironment. Analogously to mice, we observed in human patients with MS that CCL5-producing bT_{RM} localized at higher density in $MHCII^+$ areas corresponding to preactive lesions. These results

[1]Department of Pathology and Immunology, University of Geneva, 1211 Geneva, Switzerland. [2]Division of Clinical Pathology, Geneva University Hospital, 1211 Geneva, Switzerland. [3]Department of Neuropathology, University of Göttingen Medical Center, 37075 Göttingen, Germany. [4]Klinikum rechts der Isar, Department of Experimental Neuroimmunology, Technical University Munich, 81675 Munich, Germany. [5]Munich Cluster of Systems Neurology (SyNergy), 80539 Munich, Germany. [6]Mintaka Foundation for Medical Research, 1205 Geneva, Switzerland. [7]Department of Biomedicine–Haus Petersplatz, University of Basel, 4031 Basel, Switzerland.
*Corresponding author. Email: doron.merkler@unige.ch

provide a mechanistic insight into how viral CNS infection at a young age can predispose to autoimmune diseases later in life.

RESULTS

Viral infection in EL predisposes the brain for autoimmunity

To determine the age-dependent association of brain infection with autoimmunity, we modified the previously described intracranial rLCMV infection model of adult mice to reproduce EL infection. We infected 1-week-old mice with rLCMV intracerebrally and compared them to mice infected at the age of 3 to 4 weeks [hereafter referred to as young adults (YA); fig. S1A]. Intracerebral infection in EL or as YA induced similar expansion of virus-specific antiviral $CD8^+$ T cells (fig. S1B), and in both experimental settings, virus loads were reduced to background within 5 weeks after infection, as determined by quantitative real-time polymerase chain reaction (RT-PCR; fig. S1C). Subsequently, we transferred in vitro–activated myelin oligodendrocyte glycoprotein $(MOG)_{35–55}$–specific T cell receptor (2D2 TCR)–transgenic $CD4^+$ T cells intraperitoneally into virus-cleared mice or age-matched mock-infected controls (Fig. 1A and fig. S2A). These autoreactive 2D2 T cells react against the $MOG_{35–55}$ peptide expressed by oligodendrocytes and thus have the capacity to precipitate experimental autoimmune encephalomyelitis (EAE) (*30*). Regardless of age during viral infection, mice that received 2D2 T cells developed classical symptoms of EAE, such as hindlimb paresis and paralysis, at levels comparable to those of their age-matched mock-infected controls (fig. S2, B and C). Accordingly, expansion of transferred T cells both in the blood (fig. S2D) and recruited to the spinal cord (fig. S2E) was comparable and resulted in similar numbers of spinal cord EAE lesions (fig. S2, F and G). However, mice that had been infected in EL showed an increased incidence (Fig. 1B) and severity (Fig. 1, C and D) of atypical symptoms (see Materials and Methods) compared to age-matched mock-infected controls, a phenomenon that was not observed when mice had been infected as YA (Fig. 1, E to G). In accordance with the atypical symptoms, we observed an increased recruitment of transferred $CD45.1^+$ congenic 2D2 T cells to the cerebrum (forebrain)

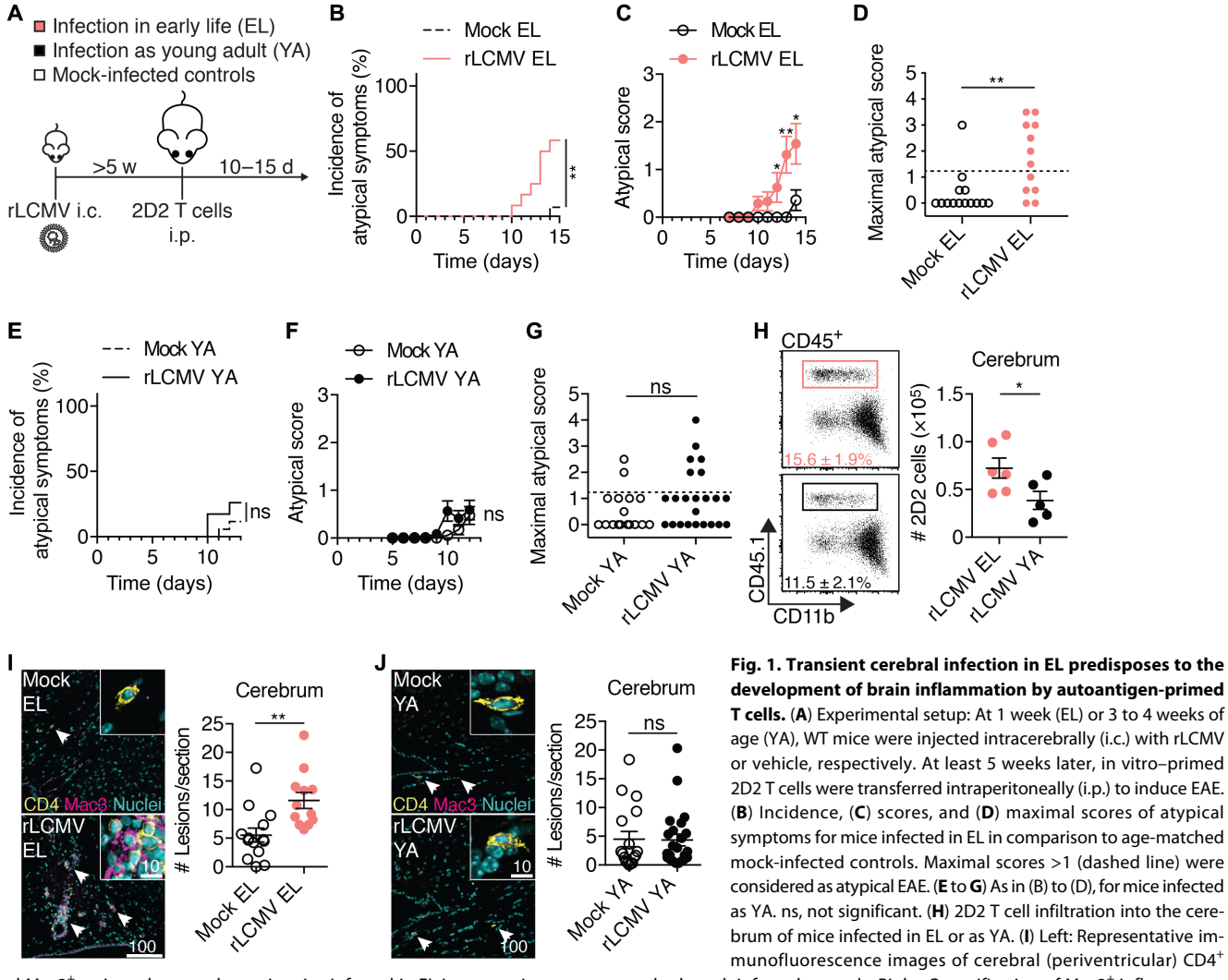

Fig. 1. Transient cerebral infection in EL predisposes to the development of brain inflammation by autoantigen-primed T cells. (**A**) Experimental setup: At 1 week (EL) or 3 to 4 weeks of age (YA), WT mice were injected intracerebrally (i.c.) with rLCMV or vehicle, respectively. At least 5 weeks later, in vitro–primed 2D2 T cells were transferred intraperitoneally (i.p.) to induce EAE. (**B**) Incidence, (**C**) scores, and (**D**) maximal scores of atypical symptoms for mice infected in EL in comparison to age-matched mock-infected controls. Maximal scores >1 (dashed line) were considered as atypical EAE. (**E** to **G**) As in (B) to (D), for mice infected as YA. ns, not significant. (**H**) 2D2 T cell infiltration into the cerebrum of mice infected in EL or as YA. (**I**) Left: Representative immunofluorescence images of cerebral (periventricular) $CD4^+$ T cells and $Mac3^+$ activated macrophages in mice infected in EL in comparison to age-matched mock-infected controls. Right: Quantification of $Mac3^+$ inflammatory lesions. (**J**) As in (I), for mice infected as YA. Symbols represent individual mice, except for (C) and (F), where data represent means ± SEM ($n = 12$ to 23 mice per group). Data are pooled (B to G, I, and J) or representative (H) of two independent experiments. $^*P < 0.05$, $^{**}P < 0.01$, log-rank (Mantel-Cox) test (B and E), Mann-Whitney *U* test (C, D, F, and G), and Student's *t* test (H to J).

in mice that had been infected in EL (Fig. 1H and fig. S2H). Further, histopathological analysis revealed a significantly ($P = 0.0032$) higher number of cerebral EAE lesions containing $CD4^+$ T cell and activated ($Mac3^+$) macrophages in mice that had been infected in EL compared to mock-infected control animals (Fig. 1I), a phenomenon that was not seen in mice that had been infected as YA (Fig. 1J). Independently of the age of infection and CNS region analyzed, 2D2 T cells displayed a T helper type 1 (T_H1) phenotype, as evidenced by intracellular expression of interferon-γ (IFN-γ) and absence of interleukin-17A (IL-17A; fig. S2, I and J). Together, these results indicate that transient infection of the brain in EL fosters the generation of autoimmune lesions in the brain.

Brain autoimmune lesions precipitate close to sites of previously resolved infection

Next, we examined the spatial association between brain areas that had previously been exposed to viral infection and the occurrence of cerebral EAE lesions. To trace virus spread, we infected LoxP-flanked red fluorescent protein (RFP) reporter (St-RFP) mice with rLCMV-expressing Cre recombinase (rLCMV-Cre; fig. S3A). rLCMV-Cre infection irreversibly induces reporter gene expression in virus-experienced cells (*26*, *27*). As observed for viral RNA, no viral protein (fig. S3B) could be detected 5 weeks after infection. However, virus-purged RFP-expressing (RFP^+) reporter cells were still detectable around the brain ventricles and in the corpus callosum of adult mice that had been infected in EL but not in mice that had been infected as YA (fig. S3, B to D). This is consistent with a partial non-cytolytic virus clearance mechanism occurring after EL rLCMV infection, whereas later infection results in complete elimination of virus-infected cells. Immunofluorescence costaining of RFP^+ cells in adult St-RFP mice that had been infected with rLCMV-Cre in EL revealed virus-purged RFP^+ cells that were found in the ependymal linings and adjacent parenchyma, including neurons and glial cells (fig. S3E). After 2D2 T cell transfer into these mice (Fig. 2A), most (74%) of cerebral EAE lesions were either colocalized with RFP^+ reporter cells or found in their close proximity (<400 μm; Fig. 2B). The measured distances between EAE lesions and RFP^+ reporter cells were significantly lower than the distances obtained from a computer simulation of randomly distributed EAE lesions ($P < 0.0001$; Fig. 2C). Together, this ascertains a spatial association between brain autoimmune lesions and areas of previous virus infection.

To investigate whether virus-purged RFP^+ cells could represent a potential source of persisting but not detectable virus antigen that could be essential for the development of observed EAE lesions in the cerebrum, we used iDTR mice, in which Cre-inducible expression of diphtheria toxin receptor renders cells susceptible to ablation by

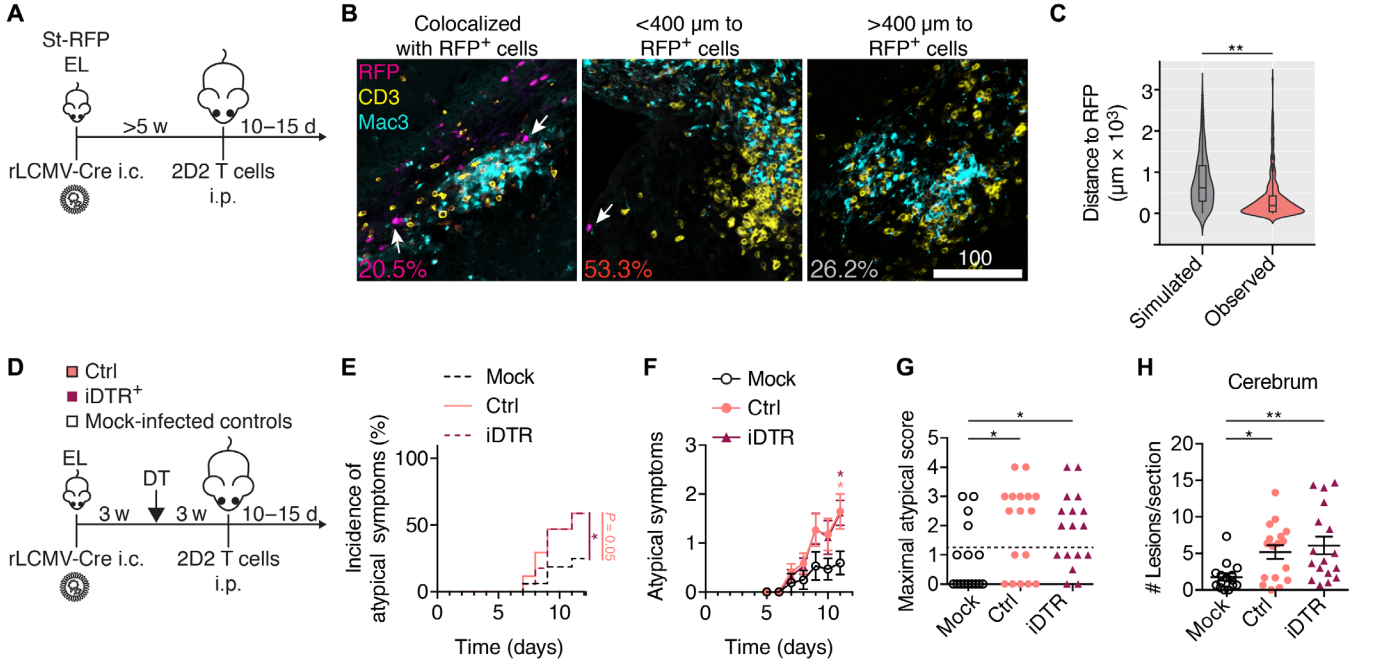

Fig. 2. Brain autoimmune lesions in mice infected in EL develop preferentially close to sites of resolved virus infection. (**A**) Experimental setup: St-RFP mice were infected intracerebrally with rLCMV-Cre in EL, and in vitro–primed 2D2 T cells were transferred >5 weeks after infection. (**B**) Representative images of lesions containing T cells (CD3) and activated macrophages (Mac3) with RFP^+ reporter cells 2 weeks after transfer of 2D2 T cells. Numbers indicate the percentage of lesions found colocalized with or in indicated distance to RFP^+ cells. (**C**) Spatial correlation analysis of lesions and RFP^+ cells. Number of lesions in correlation to distances to the closest RFP^+ cells are presented in comparison to a computer-simulated random distribution. Data show a spatial analysis of a total of $n = 351$ lesions ($n = 10$ mice) compared to $n = 354$ simulated random lesions. Distances are represented as boxplots (with boxes indicating the 25 to 75% interquartile range) and surrounded by violin plots. (**D**) Experimental setup for (E) to (H): Cre recombinase–inducible DTX receptor (iDTR) mice were infected intracerebrally with rLCMV-Cre. Virus-experienced cells were ablated by diphtheria toxin (DTX) administration 3 weeks before transfer of 2D2 T cells. (**E**) Incidence, (**F**) scores, and (**G**) maximal scores of atypical symptoms of ablated iDTR mice in comparison to DTX-treated infected WT littermates and mock-infected controls. Maximal scores >1 (dashed line) were considered as atypical EAE. Data in (F) represent means ± SEM ($n = 15$ to 17 mice per group). (**H**) Histological analysis of cerebral inflammation ($Mac3^+$ lesions) 2 weeks after 2D2 T cell transfer. Symbols represent individual mice, and means ± SEM are shown. All data are pooled from two independent experiments. *$P < 0.05$, **$P < 0.01$, Mann-Whitney *U* test (C), log-rank (Mantel-Cox) tests against mock-infected controls (E), Kruskal-Wallis *H* test (F and G), and one-way analysis of variance (ANOVA) (H).

administration of diphteria toxin (DTX). We infected iDTR mice with rLCMV-Cre in EL and depleted virus-experienced cells by administration of DTX 3 weeks later (Fig. 2D). rLCMV-Cre infection in St-RFP–iDTR double transgenic mice confirmed that DTX administration eliminated >95% of virus-purged RFP^+ cells (fig. S4, A and B), but this treatment did not alter the development of classical EAE and spinal cord inflammation (fig. S4, C to E). Neither did the depletion of virus-purged cells protect mice from the development of atypical symptoms or reduce the number of cerebral lesions (Fig. 2, E to H). This indicates that the existence of virus-purged cells alone is not sufficient to explain the development of cerebral EAE lesions and corresponding symptoms after 2D2 T cell transfer.

CCL5-producing bT_{RM} generated after infection in EL predispose to brain autoimmunity

Given the spatial but noncausal relationship of cerebral EAE lesions and virus-purged cells, we next characterized the inflammatory tissue microenvironment of RFP^+ reporter cells. We compared the expression of inflammation-related genes in tissue punches from brain areas containing RFP^+ reporter cells obtained from adult mice that had been infected in EL with equivalent brain areas from mock-infected control animals and adult mice that had been infected as YA (Fig. 3A). Gene expression patterns of virus-purged mice that had been infected as YA clustered together with mock-infected controls, whereas a distinct gene expression pattern was obtained from mice that had been infected in EL (Fig. 3B). This expression pattern indicated persistent expression of several proinflammatory genes, including the chemokine *Ccl5* as compared to a pool of both control groups (Fig. 3C). Immunohistochemical analysis identified the majority (83.0 ± 3.5%) of $CCL5^+$ cells in these areas as $CD3^+$ T cells (Fig. 3D and fig. S5A). We did not observe any overlap (<1%) of CCL5 staining with $GFAP^+$ astrocytes, Nogo-A^+ oligodendrocytes, or $NeuN^+$ neurons (fig. S5A), indicating that CCL5 expression was mostly restricted to leukocytes. More detailed flow cytometric analysis identified 88.6 ± 0.6% of $CCL5^+$ leukocytes as $CD3^+$ T cells (fig. S5B). Brain-derived CD11b high-expressing macrophages/microglia or $NK1.1^+$ natural killer cells represented only 1.1 ± 0.1% or 2.1 ± 0.1% of $CCL5^+$ leukocytes, respectively. Among $CD3^+$ T cells, $CD8^+$ bT_{RM} were the major producers of CCL5 in adult mice infected in EL (71.1 ± 1.3%), whereas brain-resident $CD4^+$ T cells made a smaller contribution (20.9 ± 1.3%; Fig. 3E and fig. S5B). Regardless of age during previous infection, bT_{RM} of adult mice had a comparable phenotype with respect to bona fide bT_{RM} markers CD69 and granzyme B (*13*) (fig. S6, A to C) but were more numerous in adult mice that had been infected in EL as measured by flow cytometry (fig. S6D). Numbers of $CCL5^+$ bT_{RM} in adult mice were significantly increased in adult mice that had been infected in EL compared to mice that had been infected as YA ($P = 0.0092$; Fig. 3F), but the frequencies of CCL5 expression in bT_{RM} in the two groups (57 ± 2% and 55 ± 2%, respectively) were not significantly different ($P = 0.48$; Fig. 3, G and H). In contrast to bT_{RM}, only a small proportion of splenic memory T cells (T_M) expressed CCL5 (fig. S6, E and F), and numbers of splenic $CCL5^+$ T_M in mice were comparable between mice that had been infected in EL or as YA (fig. S6G). In addition, $CCL5^+$ and $CCL5^-$ bT_{RM} localized at a higher density in proximity (<200 μm) to RFP^+ reporter cells in mice that had been infected in EL (Fig. 3I and fig. S6H). This accumulation led to the formation of T_{RM} clusters, which were observed in the brains of mice that had been infected in EL but rarely in mice infected as YA (Fig. 3J). Depletion of RFP^+ reporter cells (compare Fig. 2 and fig. S5) did not reduce T_{RM} numbers or clusters (fig. S6, I and J), indicating that virus-purged cells are not required for their maintenance.

CCL5 is mainly involved in the recruitment of T cells and macrophages via chemokine receptor CCR5 (*31*). To test whether CCL5, also known as RANTES, is essential for the observed EAE phenotype, we treated virus-purged animals with the potent CCR5 antagonist 5P12-RANTES (*32*) after transfer of 2D2 T cells (Fig. 3K). 5P12-RANTES is an analog of human CCL5 that potently blocks CCR5 (fig. S7A) without affecting signaling on CCR1 or CCR3 (fig. S7, B and C). Treatment with 5P12-RANTES did not affect the development of classical EAE symptoms and spinal cord inflammation (fig. S8), but it abrogated the development of atypical EAE symptoms (Fig. 3, L to N) and reduced the number of cerebral lesions to amounts of mock-infected controls (Fig. 3O). Together, these data suggest that $CCL5^+$ bT_{RM} clusters at sites of previous infection constitute a critical component of the persistent proinflammatory environment that contributes to the recruitment of $CCR5^+$ autoreactive T cells and monocytes to the brain.

bT_{RM} and $MHCII^+$ antigen-presenting cells mark areas prone to develop autoimmune lesions

Because encephalitogenic $CD4^+$ T cells require reactivation by antigen-presenting cells (APCs) during brain invasion (*33*), we next investigated the presence of APCs at sites of previous transient infection in the brain using MHCII as marker. Adult mice that had been infected in EL revealed $MHCII^+$ APCs in the brain parenchyma, whereas MHCII expression was almost completely absent from the brain parenchyma in mice that had been infected as YA and in mock-infected control animals (Fig. 4A). MHCII expression colocalized with $iba1^+$ microglia/macrophages (94 ± 2%; Fig. 4B) and was found in significantly higher density in the vicinity (<200 μm) of RFP^+ cells ($P = 0.0088$; Fig. 4C), similar to what was observed for bT_{RM}. $MHCII^+$ APCs and $CD8^+$ T cells frequently clustered together in the brain parenchyma, and such clusters were significantly more frequent in adult mice infected in EL than in mice infected as YA ($P = 0.0002$; Fig. 4D). As for bT_{RM}, parenchymal MHCII expression was not affected by the depletion of virus-purged cells (fig. S9).

In normal-appearing white matter (NAWM) of MS brains, clusters of $CD68^+$ phagocytes expressing MHCII represent a prestage to inflammatory lesions (*34*). Thus, we investigated the localization and phenotype of $MHCII^+$ APCs and bT_{RM} in human tissue samples from patients with MS. We could identify such nondemyelinated areas containing human leukocyte antigen gene complex class II (HLA-DR) high-expressing areas in 7 of 8 investigated MS autopsies (9 of 10 analyzed tissue samples), whereas only 4 of 16 control autopsies [non-neurological disease (NND)] showed this feature (7 of 30 analyzed tissue samples; Fig. 5, A and B, and table S1). In MS tissue samples, HLA-DR high-expressing areas displayed a significantly higher density of $CD8^+$ T cells when compared to HLA-DR low-expressing areas ($P = 0.0017$), whereas $CD8^+$ T cell numbers were not significantly increased in HLA-DR high-expressing areas in NND control samples ($P = 0.83$; Fig. 5C). Multiplexed immunofluorescence costaining for CCL5, CD8, CD69, B cell lymphoma 2 (BCL-2), and $CD68^+$ cells on brain sections (Fig. 5D) revealed that most $CD8^+$ cells identified are bona fide T_{RM} ($CD8^+CD69^+BCL\text{-}2^+$) in brain samples of patients with MS (90.3 ± 1.6%) and of NND (85.3 ± 1.9%; Fig. 5E). Comparison of relative densities of $CD8^+$ T cell subsets between HLA-DR low- and high-expressing areas in the same tissue sample

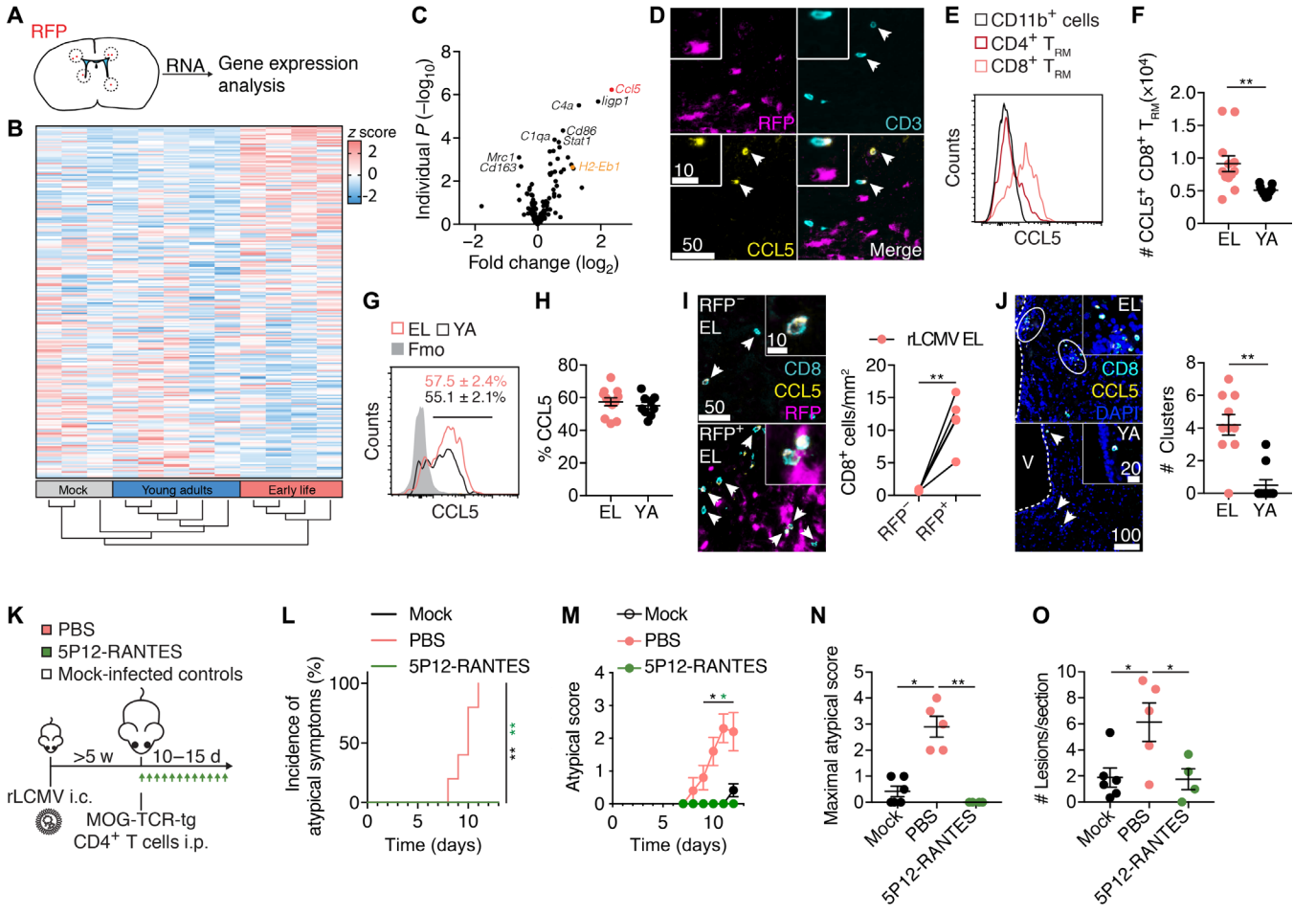

Fig. 3. Clustering of CCL5$^+$ T$_{RM}$ at sites of previous infection leads to high local CCL5 expression that confers enhanced vulnerability to autoimmune attack. (**A**) Schematic representation of tissue sampling around RFP$^+$ reporter cells for transcriptome analysis. (**B**) Gene expression analysis of 256 inflammatory genes represented as heatmap. (**C**) Volcano plot of gene expression data presented in (B). Mice that had been infected in EL are compared to the pool of both control groups (mock-infected and infected as YA). (**D**) Representative image illustrating CCL5 expression by CD3$^+$ T cells. (**E** to **H**) Ex vivo flow cytometric analysis of CCL5 expression. (E) Representative histograms of intracellular staining for CCL5 in brain CD8$^+$CD69$^+$CD44$^+$ T$_{RM}$ and CD4$^+$CD69$^+$CD44$^+$ T$_{RM}$ >5 weeks after EL intracerebral rLCMV infection in comparison to CD11b$^+$ microglia/macrophages in adult mice infected in EL. (F) Numbers of CCL5$^+$ brain T$_{RM}$ persisting at 5 weeks after intracerebral rLCMV infection. (G and H) Comparison of CCL5 expression in CD8$^+$ bT$_{RM}$ from adult mice infected in EL or as YA. Fmo, fluorescence minus one. (**I**) Left: Representative images of CCL5$^+$CD8$^+$ T cells in areas with (RFP$^+$) and without (RFP$^-$) reporter cells. Right: Quantification of CD8$^+$ T cell density in RFP$^+$ areas (<200 μm to RFP$^+$ cells) in correlation to RFP$^-$ areas. (**J**) Left: Representative images of CD8$^+$CCL5$^+$ T cell clusters in adult mice infected in EL (top) and as YA (bottom). Right: Quantification of CD8$^+$ T cell clusters (>4 CD8$^+$ T cells in a field of view of 0.04 mm^2) on brain tissue sections in three different anatomical areas. DAPI, 4′,6-diamidino-2-phenylindole. (**K**) Experimental setup for (L) to (O): Mice were infected intracerebrally with rLCMV in EL or as YA, and in vitro–primed 2D2 T cells were transferred >5 weeks later. Mice were treated intraperitoneally with 10 μg of 5P12-RANTES or phosphate-buffered saline (PBS) daily after transfer of 2D2 T cells. (**L**) Incidence, (**M**) scores, and (**N**) maximal scores of atypical EAE in 5P12-RANTES–treated mice in comparison to PBS-treated littermates or mock-infected controls. (**O**) Histological analysis of cerebral inflammation (Mac3$^+$ lesions) 2 weeks after 2D2 T cell transfer of mice in (L) to (N). (F, H, I, J, N, and O) Symbols represent individual mice. (M) Means ± SEM is shown ($n = 4$ to 6 mice per group). Gene expression profiling (B and C) was performed once. Other data are either pooled (F, H, and J) or representative (D, E, I, L, and O) of two independent experiments. *$P < 0.05$, **$P < 0.01$, Student's t test (F and H), paired Student's t test (I), Mann-Whitney U test (J), log-rank (Mantel-Cox) test (L), Kruskal-Wallis H test (M and N), and one-way ANOVA (O).

revealed that both CCL5$^-$ and CCL5$^+$ T$_{RM}$ were preferentially located in HLA-DR high-expressing NAWM of preactive MS lesions (Fig. 5F). CCL5$^+$ T$_{RM}$, but not CCL5$^-$ T$_{RM}$, were also increased in the rare HLA-DR high-expressing areas in control samples (Fig. 5G).

Together, our experimental data suggest that transient brain virus infection in EL can generate a long-lived proinflammatory microenvironment containing CCL5-producing bT$_{RM}$ and MHCII$^+$ APCs, which fosters the generation of autoimmune lesions in the brain. Analogously to mice, the positioning of CCL5$^+$ bT$_{RM}$ in the vicinity of MHCII$^+$ APCs in NAWM may thus point toward areas prone to the development of MS lesions in humans.

DISCUSSION

In the current work, we provide evidence that virus-induced long-lived bT$_{RM}$ generated in EL can promote a durable fertile field in the brain that serves as a gateway for circulating autoreactive T cells into the tissue. This increased susceptibility of the brain to an autoimmune attack was mediated by CCL5, for which bT$_{RM}$ served as an important cellular source. Further, these CCL5$^+$ bT$_{RM}$ were preferentially situated in close vicinity to MHCII$^+$ APCs. Our study has several implications: First, autoreactive T cells that have escaped negative selection in the thymus are frequently detected in human blood of healthy individuals (*35*, *36*) but only rarely induce

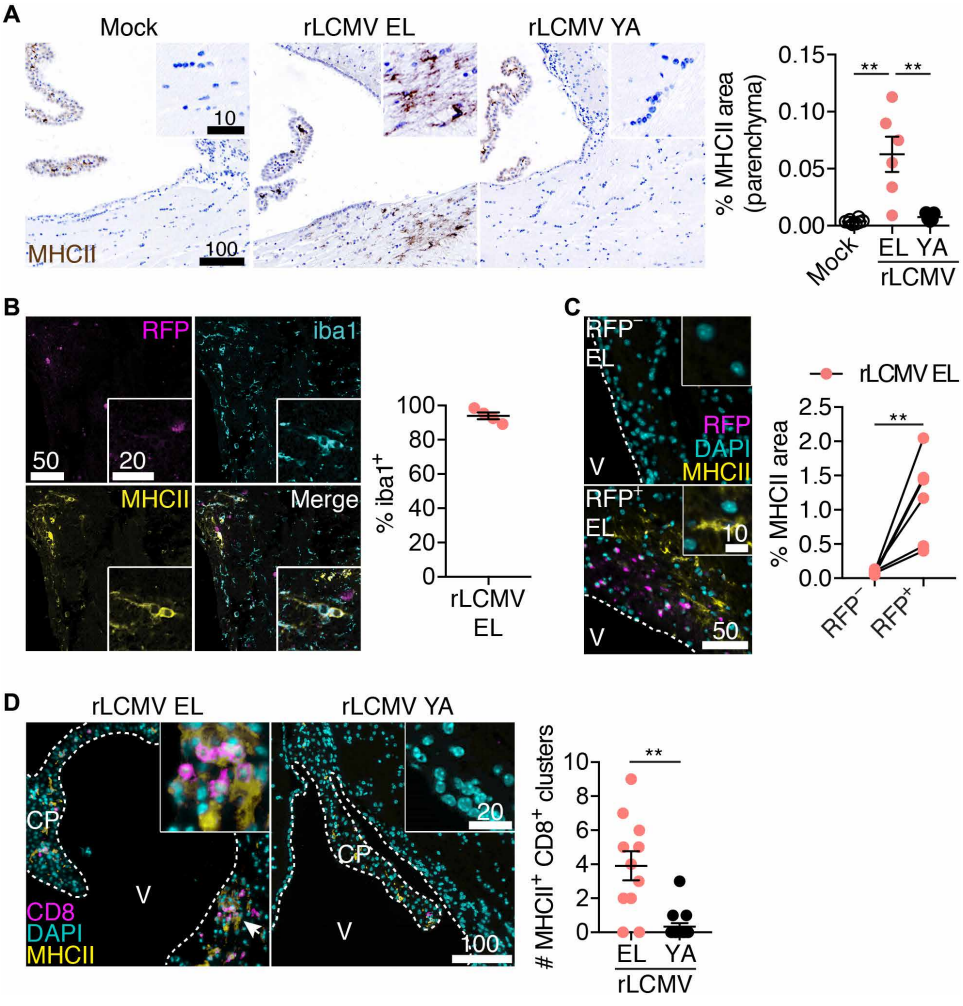

Fig. 4. bT_{RM} cluster with $MHCII^+$APCs in postinfectious mice. WT mice were infected with rLCMV intracerebrally in EL or as YA and colocalization of $CD8^+$ T cells, and $MHCII^+$ APCs was analyzed >5 weeks later. Mock-infected control mice were injected with vehicle only. (**A**) Left: Representative images of cerebral MHCII expression in the choroid plexus and periventricular brain parenchyma. Right: Quantification of parenchymal MHCII expression, persisting >5 weeks after infection ($n = 4$ to 6). (**B**) Representative image and quantification of $iba1^+$ $MHCII^+$ cells in proximity to virus-purged RFP^+ cells ($n = 4$). (**C**) Left: Representative images of $MHCII^+$ cells in areas with (RFP^+) and without (RFP^-) reporter cells. Right: Quantification of MHCII expression in RFP^+ areas (<200 μm to RFP^+ cells) in correlation to RFP^- areas ($n = 6$). (**D**) Left: Representative images of $CD8^+$ T cell clustering with $MHCII^+$ APCs in adult mice infected in EL and as YA. Right: Quantification of $MHCII^+$ $CD8^+$ T cell clusters (>4 $CD8^+$ T cells in an $MHCII^+$ field of view of 0.04 mm^2) on brain tissue sections on three different anatomical areas ($n = 11$ to 15). Symbols represent individual mice, and means ± SEM is indicated in (A), (B), and (D). Data are either pooled (D) or representative (A to C) of two independent experiments. $^{**}P < 0.01$, one-way ANOVA (A), followed by Tukey's multiple comparisons test, paired Student's *t* test (C), and Mann-Whitney *U* test (D).

autoimmune disease (*37*). Our findings of CCL5-producing bT_{RM} clusters at sites of previous infection thus might explain how the brain can become permissive to autoreactive T cells from the circulation as a long-term consequence of a transient viral infection. Under physiological conditions, such immune cell recruitment to the brain is highly limited by the blood-brain and blood–cerebrospinal fluid barriers that physically separate the brain parenchyma from circulating immune cells (*38*). As a result, the immune system can remain largely ignorant toward a persisting virus infection in the CNS (*8*). Further, transgenic mouse models expressing TCRs specific for MHCI-restricted CNS antigen do not usually develop spontaneous autoimmune disease without peripheral priming of antigen-specific T cells in an infectious context (*39*, *40*). Second, low expression of MHC molecules, especially MHCII, in the brain parenchyma usually restricts reactivation of patrolling effector or effector T_M specific for CNS antigen (*37*). Thus, the generation of clustered $CCL5^+$ bT_{RM} that persist close to $MHCII^+$ APCs could enable the reactivation of such recruited MHCII-restricted autoreactive T cells, which subsequently precipitate an inflammatory autoimmune lesion.

As an independent finding, our study documents that upon infection in EL, a proportion of virus-infected cells in the brain is cleared in a noncytolytic manner. We harnessed this particularity, which enabled us to detect virus-purged cells and thus to track brain areas that had previously been a site of virus infection. Why noncytolytic virus clearance was exclusively observed after EL infection but not when virus was encountered later in life remains unknown at present time. Noncytolytic clearance has been documented for several viruses from the brain (*41*, *42*), as well as from other organs (*43*–*45*). For instance, T cell–derived IFN-γ was shown to primarily mediate noncytolytic Sindbis virus clearance from neurons (*41*). Although the exact conditions favoring either cytolytic or noncytolytic clearance remain to be elucidated, it is tempting to speculate that glial cells infected in EL are more resistant to lytic effector mechanisms than their adult counterparts. Alternatively, it is also possible that differences in innate and adaptive antiviral responses may favor one of the two outcomes. Noncytolytic virus clearance has been reported to take place under conditions in which the numerical ratio between T cells and infected cells is low (*45*). It is thus possible that infection of the brain in EL may have posed a greater challenge for infiltrating virus-specific $CD8^+$ T cells. This may also explain why we found an increased number of bT_{RM} clusters after infection in EL. However, depletion of virus-purged cells per se did reduce neither bT_{RM} clusters nor MHCII expression on APCs, nor did it alter the susceptibility of autoimmune brain lesions. Instead, the clustering of CCL5-expressing bT_{RM} was essential for the precipitation of autoimmune brain lesions. In principle, most cells in the body have the ability to express CCL5 upon exposure to inflammatory signals. CCL5 is induced by nuclear factor κB and interferon receptor signaling during acute infection but relies on continuous signaling to maintain expression (*46*, *47*). However, in T cells, CCL5

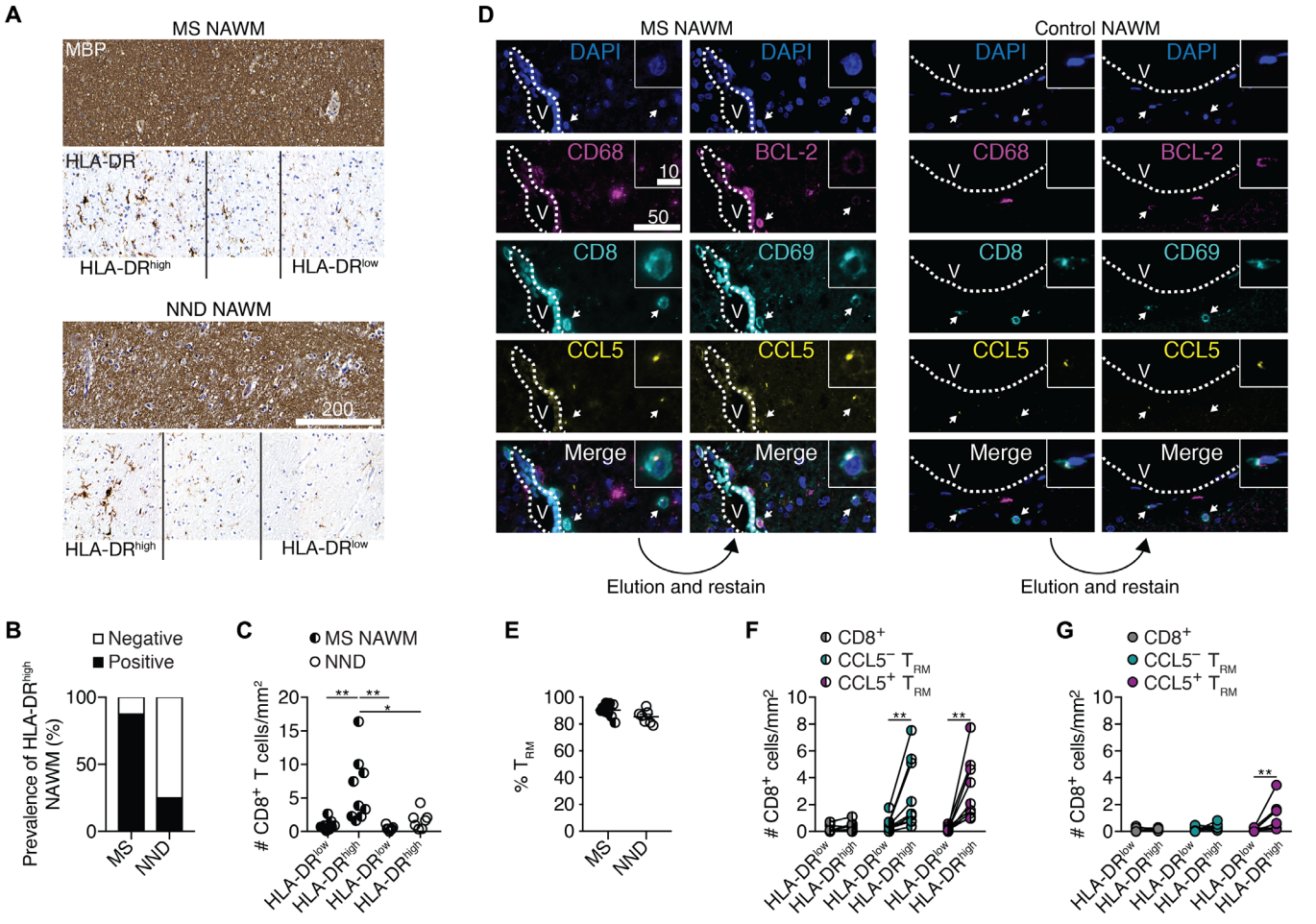

Fig. 5. bT$_{RM}$ cluster in HLA-DR high-expressing preactive MS lesions. (**A**) Cerebral tissue sections of patients with MS and controls (NND) were stained for myelin basic protein (MBP) and HLA-DR to identify HLA-DR high-expressing (HLA-DR^{high}) and low-expressing (HLA-DR^{low}) NAWM. (**B**) Prevalence of HLA-DR^{high} NAWM in investigated cases. (**C**) Quantification of CD8$^+$ T cells in HLA-DR^{high} areas in comparison to HLA-DR low-expressing (HLA-DR^{low}) areas in NAWM of patients with MS and NND control samples. Symbols represent individually analyzed tissue areas of $n = 9$ MS tissue samples and $n = 7$ NND controls. (**D**) Representative images illustrating the identification of CCL5$^+$ T$_{RM}$ (CD8$^+$CD69$^+$BCL-2$^+$) in HLA-DR^{high} areas using an elution and restain approach (for details, see Material and Methods). Left: MS NAWM; right: NND NAWM. (**E**) Quantification of T$_{RM}$ (CD8$^+$CD69$^+$BCL-2$^+$) among CD8$^+$ cells. (**F**) Quantification of CD8$^+$ (non-T$_{RM}$, CD8$^+$CD69/BCL-2$^-$), CCL5$^-$, and CCL5$^+$ T$_{RM}$ in HLA-DR^{high} and HLA-DR^{low} areas in NAWM of patients with chronic MS. (**G**) Quantification of CD8$^+$ (non-T$_{RM}$), CCL5$^-$, and CCL5$^+$ T$_{RM}$ (CD8$^+$CD69$^+$BCL-2$^+$) in HLA-DR^{high} and HLA-DR^{low} areas in NAWM of control samples (NND). $^{**}P < 0.01$, $^{*}P < 0.05$, one-way ANOVA, followed by Tukey's multiple comparisons test (C), and Student's t test (E). (F and G) HLA-DR^{high} and HLA-DR^{low} areas of the same tissue sample have been compared in a matched analysis (two-way repeated-measures ANOVA, followed by Sidak's multiple comparisons test). See also table S1.

gene expression can stay constitutively activated in T$_M$ (*48*, *49*) and is induced by the transcription factor Kruppel-like factor 13 (*50*). This likely explains why after resolution of infection in the brain, we observed persisting CCL5 expression almost exclusively in T cells but not in other cell types including glial cells. CCL5 mediates the recruitment of CCR5$^+$ activated or T$_M$ and monocytes during acute infection (*31*). Persisting CCL5 in the brain could thus similarly foster the recruitment of CCR5$^+$ autoreactive T cells and macrophages. CCL5 has been described to promote adherence of autoreactive CD4$^+$ T cells to leptomeninges in the brain in an EAE model (*51*), indicating that bT$_{RM}$-derived CCL5 could allow CCR5$^+$ 2D2 T cells to overcome the physical separation from their cognate antigen by the brain's endothelial barriers and to invade the brain parenchyma and precipitate brain autoimmune inflammation. Although treatment with the CCR5 antagonist 5P12-RANTES prevented the development of brain inflammation in our model, we did not observe an effect of CCR5 blockade on the development of classical EAE. Similar pharmacological approaches such as the administration of Met-RANTES or anti-CCL5 antibodies have not ameliorated classical EAE either (*52*, *53*), and Ccr5-deficient mice are not protected from classical EAE (*54*). One possible explanation for this could be a functional redundancy of CCL5-mediated immune cell recruitment in the spinal cord but not in the brain. CCR5-mediated immune cell recruitment is necessary for the successful clearance of West Nile virus from the brain (*55*).

Besides serving as chemoattractant, CCL5 can also provide costimulatory signals to CCR5$^+$ T cells and macrophages. CCR5 signaling in T cells enhances the stability of the immunological synapse and results in increased T cell proliferation and cytokine production (*56*). In macrophages and microglia, CCL5-CCR5 signaling increases production of reactive nitric oxide (*57*–*59*). Further, CCL5-CCR5 signaling provides resistance of T cells and macrophages to apoptotic

signals (*60*, *61*). It is therefore possible that besides serving as chemoattractant, bT_{RM}-derived CCL5 contributes to the stimulation of recruited autoreactive T cells and macrophages, thereby exerting a nonredundant function in the observed long-lived fertile field.

Analogously to mice, we observed clusters of MHCII-expressing $CD68^+$ phagocytes frequently in NAWM of patients with MS and to a lower extent in corresponding control samples. In MS, such clusters are thought to represent a prestage of MS lesions (*34*, *62*), which occur before the actual development of the demyelinating lesion (*63*). In this regard, imaging studies documented alterations in NAWM, which have been speculated to correspond to preactive lesions, can precede the appearance of gadolinium-enhancing lesions on magnetic resonance imaging for months to years (*64*). Although only limited numbers of T cells are present in NAWM (*62*, *65*), we noted that bT_{RM} preferentially accumulated in preactive MS areas, suggesting that bT_{RM} are not distributed randomly but preferentially in such lesion-prone areas in the NAWM.

Beyond the CNS, similar clustering of T_{RM} together with $MHCII^+$ myeloid cells has been previously described in epithelial barriers, where it mediated CCL5-dependent recruitment and retention of $CD4^+$ T_M (*66*, *67*). Further, the formation of mixed lymphocyte clusters in the skin is a prerequisite for efficient T cell activation and elicitation of contact hypersensitivity responses (*68*). This indicates that the herein described mechanism may also be of relevance for predisposing other organs to inflammatory diseases.

Our study has several limitations. To begin with, the route of brain virus infection as performed in the current study relies on intracerebral application of the virus to ensure reproducible brain infection. However, under natural infection conditions, virus spread to the CNS frequently occurs secondary to systemic infection. Furthermore, although EAE is a widely used rodent model of MS, it does not recapitulate all features of the human disease and its pathology. In particular, activation of disease-driving autoreactive MHCII-restricted $CD4^+$ T cells may be different in EAE and MS. In our study, we induced EAE by adoptive transfer of autoreactive T_H1 cells. Whether other T_H subsets, such as, e.g., T_H17 cells, can also be recruited and activated by similar mechanisms in postinfectious brain tissue remains to be studied. In addition, the herein used mouse EAE model does not rely on B cells (*69*), which play an important role in MS (*70*). Potentially, resident memory B cells might thus equally be able to persist in the brain after a transient infection. Whether such cells could also contribute to predisposition to lesion formation has not been addressed in our study and needs further investigation.

Our histopathological analysis on human tissue provides a correlative but not a causal relationship between CCL5-expressing bT_{RM} and lesion predisposition in $HLA\text{-}DR^+$ NAWM of patients with MS. The current study was limited to a moderate case number, especially with regard to NAWM of patients with short disease duration, because such biopsies are only rarely performed. Future studies with larger cohorts of patient samples could thus bring more detailed insights into the phenotype of bT_{RM} in patients with MS in different disease stages and their potential role for disease development.

In our model, preactive clusters of bT_{RM} and $MHCII^+$ myeloid cells in the brain were induced by a transient virus infection using rLCMV. However, this does not imply a specific association of LCMV infection with an increased risk to develop MS in humans. In addition, other triggers aside from infection may also generate similar inflammatory environments. Although innate immune activation of the brain can also occur after trauma (*71*), the generation of bT_{RM} in the brain requires restimulation by their cognate antigen (*13*, *14*). In line with this, we did not observe an increased incidence of atypical EAE in mock-infected control animals that have been injected with vehicle, a procedure that is expected to result in microtrauma. Although this observation does not exclude that trauma or other sterile insults can potentially predispose the CNS for autoimmunity, this nevertheless suggests that brain infection is probably more efficient in generating the fertile fields described herein. In such a scenario of a preceding transient brain infection, the antigenic specificity of the predisposing immune response and resulting bT_{RM} remains largely irrelevant for the subsequent recruitment and reactivation of autoreactive T cells.

Therefore, our study provides explanations for two main conundrums in the interaction between viruses and autoimmunity: (i) How previous infection in a certain time window of life with several structurally unrelated viruses can be associated with an increased risk of developing disease (*3*), and (ii) how, despite this association, predisposing viral infections can elude detection as causative agents of autoimmune diseases. Demonstrating how past viral infection can lead to a durable inflammatory signature in the brain thus represents an important step toward understanding the predisposing role of environmental factors for MS and likely other autoimmune diseases.

MATERIALS AND METHODS

Study design

Our research objective was to investigate the possible relation between viral infection in EL and an enhanced susceptibility to brain autoimmune disease in adulthood. We used intracerebral infection of C57BL/6 WT mice with rLCMV as an experimental model of transient viral infection of the brain. EL infection was modeled by intracerebral infection of 1-week-old mice, whereas infection later in life was modeled by infection of YA mice (3 to 4 weeks of age). We determined susceptibility to autoimmune disease by transferring in vitro–activated, autoreactive 2D2 TCR–transgenic $CD4^+$ T cells to induce EAE in mice in previously infected mice and corresponding mock-infected controls. The development of atypical EAE symptoms and occurrence of cerebral inflammatory lesions consisting of autoreactive $CD4^+$ T cells and activated macrophages served as surrogate for brain autoimmune disease. Experiments were terminated, and data were collected when $\geq$50% of animals reached a classical EAE score of $\geq$3, which corresponded to the termination criteria defined by institutional authorities for animal experimentation.

We harnessed the fact that virus clearance in mice infected in EL was partially noncytolytic to trace sites of previous virus infection using infection of St-RFP reporter mice with rLCMV-Cre. We assessed the role of virus-purged cells by DTX-mediated ablation of these cells in iDTR mice infected intracerebrally with rLCMV-Cre. We performed gene expression analysis of sites of previous virus infection by isolating RNA from tissue stamps obtained from RFP^+ brain regions. We used immunohistochemistry and flow cytometry to identify the sources of CCL5 expression and for further investigations of the inflammatory surroundings of virus-purged RFP^+ cells. The relevance of persisting expression of the chemokine CCL5 was assessed by treatment of adult mice infected in EL with the CCR5 antagonist 5P12-RANTES during induction of EAE.

Individual group sizes for infection of mice at 1 week of age depended on litter size (5 to 10 animals). Data were pooled from two

independent experiments when it was needed for statistical power (e.g., not all animals in an experimental group developed atypical EAE). All experiments were reproduced at least once.

To assess a potential role for CCL5-expressing T_{RM} as predisposing factor for brain autoimmune disease in humans, we analyzed the presence of such cells in HLA-DR-positive NAWM of patients with MS and controls. Tissue blocks were screened for the presence of preactive NAWM by staining for HLA-DR and MBP (or Luxol fast blue). HLA-DR high-expressing areas with no signs of demyelination were included in the analysis, together with HLA-DR low-expressing or -negative areas on the same sections. Tissue blocks with excessive white matter demyelination (>30%) were excluded to limit the probability of analyzing lesion borders. A multistep dye cycling method was performed to analyze the presence of $CCL5^+$ T_{RM} (CD8 + BCL-2 + $CD69^+$) and $CD68^+$ myeloid cells on one section adjacent to the performed screening by HLA-DR and myelin staining.

Mice

C57BL/6 WT, St-RFP (*72*), Cre-iDTR (*73*), Rag1 knockout (*74*), and 2D2 TCR–transgenic mice (*30*) were bred and lodged under P2 conditions in the animal facilities of the University Medical Centre of Geneva. Sex- and age-matched mice were used for experiments. All animal experiments were authorized by the cantonal veterinary office of Geneva and performed in agreement with the Swiss law for animal protection.

Virus infection

Recombinant LCMV strains were generated according to established methods (*75*). The following virus strains were used: recombinant LCMV (rLCMV), which encodes for the glycoprotein of vesicular stomatitis virus instead of its own glycoprotein. Further, rLCMV-Cre was used. Viruses were produced, titrated, and administered to mice as previously described (*75*, *76*). For transient virus infection in the brain, 10^4 plaque-forming units of rLCMV diluted in 20 μl of minimum essential medium (Gibco) was administered intracerebrally. Mock-infected control animals were injected intracerebrally with vehicle. Brain virus load was analyzed by quantitative RT-PCR for LCMV–nucleoprotein (NP) (*77*). Brain total RNA was isolated from Hepes-glutamic acid buffer-mediated organic solvent protection effect (HOPE)–fixed tissue sections or stamps after deparaffinization using RNeasy Mini Kit (QIAGEN), complementary DNA (cDNA) was synthesized using iScript cDNA synthesis kit (Bio-Rad), and relative expression of LCMV S segment was determined against glyceraldehyde-3-phosphate dehydrogenase as housekeeping gene (QIAGEN) using iQ SYBR Green Supermix (Bio-Rad). Virus-purged cells were identified by intracerebral infection of St-RFP mice with rLCMV-Cre. Virus-purged cells were ablated in (St-RFP)xiDTR mice infected with rLCMV-Cre by administering 200 ng of DTX 2 to 3 weeks after infection for seven consecutive days.

Induction of EAE

For induction of adoptive transfer EAE, 2D2 TCR–transgenic T cells were stimulated in vitro. Splenocytes [4×10^6/ml in RPMI 1640 containing GlutaMAX and supplemented with + 10% fetal calf serum (FCS), 50 μM 2-mercaptoethanol, penicilin, and streptomycin (all from Gibco)] were stimulated with $MOG_{35–55}$ peptide (20 μg/ml) in presence of recombinant IL-2 and IL-7 (5 ng/ml; PeproTech) and split every 2 days. Six days later, cells were restimulated with plate-bound (1 μg/ml) anti-CD3 and anti-CD28 antibodies (BioLegend) in the presence of recombinant IL-12 p70 (20 ng/ml; PeproTech) and IL-18 (25 ng/ml; MBL International) for 24 hours. 2D2 TCR–transgenic T cells (1×10^6 to 2×10^6) were transferred intraperitoneally, and mice were injected with 67 ng of pertussis toxin intravenously (Sigma-Aldrich) at the time point of transfer and 2 days later. For CCR5 inhibition, animals were treated with 10 μg of 5P12-RANTES or PBS intraperitoneally daily from the time point of 2D2 T cell transfer. 5P12-RANTES was produced as previously described (*78*) and provided by the Mintaka Medical Foundation. Animals were observed daily for the development of disease, and clinical scores for classical and atypical symptoms were assigned on the basis of a five-point scale. Classical EAE was scored as follows: 0, no disease; 1, tail paralysis; 2, hindlimb paresis; 3, hindlimb paralysis; 4, forelimb and hindlimb paralysis; 5, moribund. Classical EAE was reported as means ± SEM over time. Atypical EAE was scored on the basis of a scale described previously (*79*), with some small modifications: 0, no disease; 1, scruffy appearance; 1.5, mild ataxia; 2, ataxia; 2.5, ataxia + head tilt; 3, head tilt + body leaning; 4, body rolling; 5, moribund. Animals that reached a classical or atypical score of ≥4 were immediately euthanized. Experiments were terminated when ≥50% of animals reached a classical score of ≥3. Similar to classical EAE, we report the development of atypical scores of all animals over time as means ± SEM. Because not all animals developed atypical EAE symptoms, we further report disease incidence over time and observed maximal atypical scores of all animals. To exclude a potential distortion of atypical scores by severe classical EAE symptoms, incidence of atypical EAE was taken into account when atypical EAE score was >1.

Immunohistochemistry

For staining of mouse tissue sections, the following antibodies were used: fluorescein isothiocyanate (FITC) anti-CD45.1 (A20, BioLegend), rat–anti-CD107b/Mac3 (M3/84, BioLegend), rabbit–anti-RFP (Abcam), rat–anti-CD3 (CD3-12, Bio-Rad), rabbit–anti-CD4 (D7D2Z, Cell Signaling Technology), rat–anti-LCMV (VL-4), rabbit–anti-LCMV hyperimmune serum, mouse–anti-NeuN (A60, Merck Millipore), rabbit–anti-iba1 (Wako), mouse–anti–Nogo-A (11C7), rat–anti-CD8 (4SM15, eBioscience), rat–anti-CD8 (YTS169.4), rabbit–anti-RANTES/CCL5 (25H14L17, Invitrogen), chicken–anti-GFAP (Abcam), and rat–anti-MHCII (M5/114.15.2, BioLegend). All antibodies were diluted in Dako REAL antibody diluent (Dako).

Mice were transcardially perfused with 4% paraformaldehyde (PFA). Alternatively, the brains and spleen were fixed in HOPE (DCS Innovative) fixative as previously described (*80*). Dehydrated tissues were embedded in paraffin. Between staining steps, slides were washed with wash buffer (Dako). Deparaffinized tissue sections were incubated with Dako REAL peroxidase-blocking solution (Dako) for 15 min to inactivate endogenous peroxidases. Before staining with mouse monoclonal antibodies, tissue sections were blocked with 10% mouse serum. Tissue sections were incubated with primary antibody in Dako REAL antibody diluent (Dako). For bright-field microscopic images, bound primary antibodies were visualized using peroxidase-coupled secondary antibody systems (Dako, Vector Laboratories) and polymerized 3,3′-diaminobenzidine (Dako). Nuclei were counterstained with hemalaun. For fluorescence microscopic images, bound primary antibodies were visualized either with Alexa Fluor 488–, Alexa Fluor 568–, or Alexa Fluor 647–labeled secondary antibodies or with peroxidase-labeled secondary antibodies, followed by Alexa Fluor 488 or Alexa Fluor 568 tyramide signal

amplification (TSA; Thermo Fisher Scientific). FITC anti-CD45.1 was visualized using rabbit–anti-FITC antibody (Life Technologies), followed by Alexa Fluor 488 goat–anti-rabbit antibody (Jackson ImmunoResearch). Nuclei were stained with DAPI (Invitrogen). For staining of human bright-field microscopy sections, the following antibodies were used: mouse–anti-human–CD8 (Thermo Fisher Scientific), rabbit–anti-MBP (Dako), and mouse–anti–HLA-DR (Abcam).

Between staining steps, slides were washed with wash buffer (Dako). Deparaffinized tissue sections were incubated with Dako REAL peroxidase-blocking solution (Dako) for 5 min to inactivate endogenous peroxidases and incubated with primary antibodies in Dako REAL antibody diluent (Dako). Bound primary antibodies were visualized using peroxidase-coupled secondary antibody systems (Dako) and polymerized 3,3′-diaminobenzidine (DAB, Dako). Nuclei were counterstained with hemalaun.

Multistep staining of human brain tissue

We applied a well-established and standardized dye cycling method that has been described previously and allows the staining of all six markers (BCL-2, CCL5, CD8, CD68, CD69, and DAPI) on the same tissue section (*26*, *81*). For sequential staining of $CCL5^+$ T_{RM} on human tissues sections, coverslipped deparaffinized sections were bleached over night with neutral-white 3-up light-emitting diodes (LEDSupply) at 4°C to minimize autofluorescence. Coverslips were removed in PBS at 50°C. Between staining steps, slides were washed with wash buffer (Dako). Sections were incubated with Dako REAL peroxidase-blocking solution (Dako) for 15 min to inactivate endogenous peroxidases, blocked with 10% FCS in PBS, and incubated with rabbit–anti-RANTES/CCL5 (25H14L17, Invitrogen) at 4°C overnight. After incubation with horseradish peroxidase (HRP)–labeled goat–anti-rabbit secondary antibody (Dako EnVision), staining was visualized with Alexa Fluor 488 TSA (Thermo Fisher Scientific). Slides were then stained with msIgG3–anti-CD68 (PG-M1, Dako) and msIgG1–anti-CD8 (C8/144B, Dako), followed by Alexa Fluor 555 goat–anti-msIgG1 (Life Technologies) and Atto 647 goat–anti-msIgG3 (LSBio). Slides were mounted in Fluoromount aqueous mounting medium (Sigma-Aldrich) for image acquisition. For elution of anti-CD8 and anti-CD68 stainings, slides were decoverslipped and incubated with Gendusa stripping buffer [2.5% SDS and 1% β-mercaptoethanol in 80 mM tris-HCl (pH 6.8)] for 1 hour at 50°C and washed in tab water, followed by 50% ethanol and PBS. Elution was verified under the microscope before slides were restained. TSA-amplified CCL5 staining was not eluted by this procedure. For restaining, sections were incubated with Dako REAL peroxidase-blocking solution (Dako) for 15 min, blocked with 10% FCS in PBS, and incubated with rabbit–anti-CD69 (Sigma-Aldrich) at 4°C overnight. After incubation with HRP-labeled goat–anti-rabbit secondary antibody (Dako EnVision), staining was visualized with Alexa Fluor 555 TSA (Thermo Fisher Scientific). Slides were then stained with msIgG1–anti–BCL-2 (124, Dako), followed by Alexa Fluor 647 goat–anti-msIgG1 (Life Technologies). Slides were mounted in Fluoromount aqueous mounting medium (Sigma-Aldrich) for image acquisition.

Image analysis

Immunostained sections were scanned using Pannoramic Digital Slide Scanner 250 FLASH II (3DHISTECH) in 200× magnification. Most quantifications were performed manually using Pannoramic Viewer software (3DHISTECH). Where possible, the examiner was blinded to the experimental group. For the quantification of cerebral and spinal cord EAE lesions, as well as their distance to the closest RFP^+ cell, T cell clusters and T cell–MHCII clusters, complete coronal sections obtained from at least three different tissue sections and distanced >1 mm from each other were quantified. Regions of interest (e.g., in a certain distance to RFP^+ cells) were assigned blinded to the staining results of CCL5, T cell markers, or MHCII.

DAB-revealed MHCII and RFP were automatically quantified using Definiens Developer software using a custom-made script. Computer simulation of randomly distributed lesions was performed on RFP single-stained adjacent sections to the sections used for manual quantification of lesion distance. Lesions of the average size (13,000 μm^2) and frequency (12 lesions per section) were randomly distributed using Definiens Developer software, and the distance to the closest RFP^+ cells was determined for each simulated lesion.

For representative images, white balance was adjusted, and contrast was enhanced using the tools "levels," "curves," "brightness," and "contrast" in Photoshop CS6 (Adobe). All modifications were acquired uniformly on the entire image.

Flow cytometry

For staining, the following antibodies were used: phycoerythrin (PE) anti-CCL5 (2E9/CCL5), FITC/Pacific Blue/PerCPCy5.5 anti-CD3e (145-2C11), APC/FITC/PE/PECy7 anti-CD4 (GK1.5), PE/PECy7/Brilliant Violet 605 anti-CD8a (53-6.7), Alexa Fluor 647/PerCPCy5.5/Brilliant Violet 711 anti-CD11b (M1/70), Alexa Fluor 647/Pacific Blue/Brilliant Violet 421 anti-CD11c, PerCPCy5.5/PECy7 anti-CD44 (IM7), Brilliant Violet 510/Pacific Blue anti-CD45 (30-F11), PE/Pacific Blue anti-CD45.1, Alexa Fluor 700/Brilliant Violet 711 anti-CD45.2, PerCPCy5.5 anti-CD45R/B220 (RA3-6B2), FITC anti-CD69 (H1.2F3), Alexa Fluor 647/Brilliant Violet 786 anti-CD103 (2E7), PECy7 anti-CD115, Alexa Fluor 647 anti–granzyme B (GB11), FITC anti–IFN-γ (XMG1.2), PE anti–IL-17A (TC11-18H10.1), Brilliant Violet 605 anti-Ly6C (HK1.4), Alexa Fluor 700 anti-Ly6G (1A8), Alexa Fluor 700/Brilliant Violet 605/Pacific Blue anti-MHCII (M5/114.15.2), Brilliant Violet 711 anti-NK1.1, PE anti–PD-1 (RMP1-30), FITC anti-TCRVα3.2 (RR3-16), and PE anti-TCRVβ11(KT11). For detection of virus-specific $CD8^+$ T cells, Db-$NP_{396–404}$ tetramer (TCMetrix, provided by the National Institutes of Health Tetramer Core Facility) was used.

Heparinized peripheral blood samples were incubated with antibodies for 20 min at room temperature. Erythrocytes were lysed using BD FACS (fluorescence-activated cell sorting) lysing solution (BD Biosciences). Splenocytes were collected in FACS buffer (2% FCS, 2 mM EDTA, and PBS), and erythrocytes were lysed using Red Blood Cell Lysis Buffer (BioLegend) before proceeding to staining. For the preparation of CNS leukocytes, mice were anesthetized and transcardially perfused with PBS. For some experiments, cerebra and spinal cords were stripped of meninges and processed separately. Tissues were minced, digested with Collagenase/DNase I (Roche), and homogenized using 70-μm cell strainers (BD Biosciences). Leukocytes were separated using a discontinuous Percoll gradient (30% and 70%). Surface staining was carried out with directly labeled antibodies and tetramers in FACS buffer. Isolated $CD8^+$ T cell numbers were quantified using AccuCheck Counting Beads (Invitrogen) as previously described (*82*). For ex vivo staining of CCL5 and granzyme B, cells were fixed and permeabilized using commercial

permeabilization buffer set (BioLegend). Dead cells were excluded from the analysis using Zombie Aqua Fixable Viability Kit or Zombie NIR Fixable Viability Kit (BioLegend). For intracellular staining of cytokines, isolated leukocytes were restimulated ex vivo for 4 hours at 37°C with PMA (50 ng/ml) and ionomycin (1 μg/ml; both from Sigma-Aldrich) in presence of brefeldin A (BioLegend) in RPMI 1640 containing GlutaMAX and supplemented with 10% FCS, 50 μM 2-mercaptoethanol, penicillin, and streptomycin (all from Gibco). For intracellular staining of IFN-γ and IL-17A, cells were fixed and permeabilized using commercial permeabilization buffer set (BioLegend). Dead cells were excluded from the analysis using Zombie Yellow Fixable Viability Kit (BioLegend).

Flow cytometric samples were acquired on the following cytometers: Gallios (Beckman Coulter) equipped with three lasers (blue, 488 nm; red, 633 nm; violet, 405 nm), Attune NxT cytometer (Thermo Fisher Scientific) equipped with four lasers (blue, 488 nm; yellow, 561 nm; red, 633 nm; violet, 405 nm), and LSRFortessa (BD Biosciences) equipped with five lasers (ultraviolet, 355 nm; violet, 405 nm; green, 488 nm; yellow, 561 nm; red, 640 nm) using appropriate filter sets and compensation controls. Gates were assigned according to appropriate control populations, such as fluorescence minus one stainings.

Gene expression analysis

One-millimeter tissue stamps from HOPE-fixed paraffin blocks were transferred into new blocks and cut into 5-μM slices, which were subsequently deparaffinized using isopropanol. Alternatively, full HOPE-fixed tissue sections were deparaffinized. RNA was isolated using RNeasy Mini Kit (QIAGEN). Expression profiling from tissue stamps was performed using the nCounter Nanostring Mouse Inflammation v2 Assay (NanoString Technologies). Gene expression data were analyzed using nSolver Analysis software 3.0 (NanoString Technologies).

Functional inhibition assays on chemokine receptors

Dose-dependent inhibitory activity of 5P12-RANTES was compared to that of previously described reference inhibitors for each receptor (Maraviroc for CCR5, J113863 for CCR1, and UCB35625 for CCR3) in routine assays provided by EuroscreenFAST (https://euroscreenfast.com). CCR5 inhibition was measured using an aequorin-based calcium flux assay with human MIP-1β/CCL4 as the reference agonist, and CCR1 and CCR3 inhibition was measured using radiometric assays measuring guanosine 5′-triphosphate recruitment at Gα subunits, with human RANTES/CCL5 and eotaxin/CCL11 as reference agonists, respectively.

Statistical analysis

Analysis was performed using Prism GraphPad 7.0 and 8.0. Data were tested for normal distribution. To assess significant differences between single measurements of two groups of normally distributed data, unpaired or paired two-tailed Student's *t* test was used; otherwise, Mann-Whitney *U* test was applied. To assess significant differences between more than two groups of normally distributed data, we performed one-way ANOVA, followed by post hoc analyses: Comparison against a control group was performed using Dunnet's multiple comparisons test, comparison of selected pairs of datasets was performed using Sidak's multiple comparisons test, and comparison of all pairs of datasets was performed using Tukey's multiple comparisons test. Kruskal-Wallis *H* test was applied to not normally distributed data, and post hoc analyses were corrected for multiple comparisons using Benjamini and Hochberg false discovery rate method. For comparison of disease incidence, log-rank (Mantel-Cox) test was used. A $P < 0.05$ was considered significant, and $P < 0.01$ was considered highly significant, whereas $P > 0.05$ was considered statistically not significant. Group sizes and specific statistical tests performed are stated in the corresponding figure legends. Where possible, obtained single values from every experimental animal or analyzed human tissue sample are represented. No outliers were removed.

SUPPLEMENTARY MATERIALS

stm.sciencemag.org/cgi/content/full/11/498/eaav5519/DC1

Fig. S1. Transient intracerebral infection with rLCMV in EL and as YA.
Fig. S2. Transient intracerebral infection with rLCMV does not alter $CD4^+$ T cell–driven spinal cord inflammation and classical EAE symptoms.
Fig. S3. Virus-purged cells in adult mice that had been infected in EL mark sites of previous infection.
Fig. S4. DTX-mediated ablation of virus-purged cells.
Fig. S5. T cells are the major producers of CCL5.
Fig. S6. Characterization of T_M subsets in mice infected in EL and as YA.
Fig. S7. 5P12-RANTES is a potent and selective inhibitor of CCR5.
Fig. S8. CCR5 antagonization does not alter classical EAE symptoms and spinal cord inflammation.
Fig. S9. Ablation of purged cells does not reduce MHCII expression in the brain.
Table S1. Human brain tissue samples for CD8 quantification and multiplex staining.
Table S2. Raw data.

REFERENCES AND NOTES

1. S. E. Baranzini, J. Mudge, J. C. van Velkinburgh, P. Khankhanians, I. Khrebtukova, N. A. Miller, L. Zhang, A. D. Farmer, C. J. Bell, R. W. Kim, G. D. May, J. E. Woodward, S. J. Caillier, J. P. McElroy, R. Gomez, M. J. Pando, L. E. Clendenen, E. E. Ganusova, F. D. Schilkey, T. Ramaraj, O. A. Khan, J. J. Huntley, S. Luo, P.-y. Kwok, T. D. Wu, G. P. Schroth, J. R. Oksenberg, S. L. Hauser, S. F. Kingsmore, Genome, epigenome and RNA sequences of monozygotic twins discordant for multiple sclerosis. *Nature* **464**, 1351–1356 (2010).
2. D. R. Getts, E. M. L. Chastain, R. L. Terry, S. D. Miller, Virus infection, antiviral immunity, and autoimmunity. *Immunol. Rev.* **255**, 197–209 (2013).
3. C. Münz, J. D. Lünemann, M. T. Getts, S. D. Miller, Antiviral immune responses: Triggers of or triggered by autoimmunity? *Nat. Rev. Immunol.* **9**, 246–258 (2009).
4. J. F. Kurtzke, Epidemiologic evidence for multiple sclerosis as an infection. *Clin. Microbiol. Rev.* **6**, 382–427 (1993).
5. R. S. Fujinami, M. G. von Herrath, U. Christen, J. L. Whitton, Molecular mimicry, bystander activation, or viral persistence: Infections and autoimmune disease. *Clin. Microbiol. Rev.* **19**, 80–94 (2006).
6. S. D. Miller, C. L. Vanderlugt, W. S. Begolka, W. Pao, R. L. Yauch, K. L. Neville, Y. Katz-Levy, A. Carrizosa, B. S. Kim, Persistent infection with Theiler's virus leads to CNS autoimmunity via epitope spreading. *Nat. Med.* **3**, 1133–1136 (1997).
7. C. Casiraghi, I. Shanina, S. Cho, M. L. Freeman, M. A. Blackman, M. S. Horwitz, Gammaherpesvirus latency accentuates EAE pathogenesis: Relevance to Epstein-Barr virus and multiple sclerosis. *PLOS Pathog.* **8**, e1002715 (2012).
8. D. Merkler, E. Horvath, W. Bruck, R. M. Zinkernagel, J. del la Torre, D. D. Pinschewer, "Viral déjà vu" elicits organ-specific immune disease independent of reactivity to self. *J. Clin. Invest.* **116**, 1254–1263 (2006).
9. M. G. von Herrath, R. S. Fujinami, J. L. Whitton, Microorganisms and autoimmunity: Making the barren field fertile? *Nat. Rev. Microbiol.* **1**, 151–157 (2003).
10. R. Hasbun, N. Rosenthal, J. M. Balada-Llasat, J. Chung, S. Duff, S. Bozzette, L. Zimmer, C. C. Ginocchio, Epidemiology of meningitis and encephalitis in the United States, 2011-2014. *Clin. Infect. Dis.* **65**, 359–363 (2017).
11. S. A. Logan, E. MacMahon, Viral meningitis. *BMJ* **336**, 36–340 (2008).
12. R. S. Klein, C. A. Hunter, Protective and pathological immunity during central nervous system infections. *Immunity* **46**, 891–909 (2017).
13. K. Steinbach, I. Vincenti, M. Kreutzfeldt, N. Page, A. Muschaweckh, I. Wagner, I. Drexler, D. Pinschewer, T. Korn, D. Merkler, Brain-resident memory T cells represent an autonomous cytotoxic barrier to viral infection. *J. Exp. Med.* **213**, 1571–1587 (2016).
14. L. M. Wakim, A. Woodward-Davis, M. J. Bevan, Memory T cells persisting within the brain after local infection show functional adaptations to their tissue of residence. *Proc. Natl. Acad. Sci. U.S.A.* **107**, 17872–17879 (2010).

15. X. Jiang, R. A. Clark, L. Liu, A. J. Wagers, R. C. Fuhlbrigge, T. S. Kupper, Skin infection generates non-migratory memory CD8$^+$ T_{RM} cells providing global skin immunity. *Nature* **483**, 227–231 (2012).
16. T. Gebhardt, L. M. Wakim, L. Eidsmo, P. C. Reading, W. R. Heath, F. R. Carbone, Memory T cells in nonlymphoid tissue that provide enhanced local immunity during infection with herpes simplex virus. *Nat. Immunol.* **10**, 524–530 (2009).
17. B. S. Sheridan, Q.-M. Pham, Y.-T. Lee, L. S. Cauley, L. Puddington, L. Lefrançois, Oral infection drives a distinct population of intestinal resident memory CD8$^+$ T cells with enhanced protective function. *Immunity* **40**, 747–757 (2014).
18. J. R. Teijaro, D. Turner, Q. Pham, E. J. Wherry, L. Lefrancois, D. L. Farber, Cutting edge: Tissue-retentive lung memory CD4 T cells mediate optimal protection to respiratory virus infection. *J. Immunol.* **187**, 5510–5514 (2011).
19. J. M. Schenkel, K. A. Fraser, V. Vezys, D. Masopust, Sensing and alarm function of resident memory CD8$^+$ T cells. *Nat. Immunol.* **14**, 509–513 (2013).
20. J. M. Schenkel, K. A. Fraser, L. K. Beura, K. E. Pauken, V. Vezys, D. Masopust, Resident memory CD8 T cells trigger protective innate and adaptive immune responses. *Science* **346**, 98–101 (2014).
21. J. Machado-Santos, E. Saji, A. R. Tröscher, M. Paunovic, R. Liblau, G. Gabriely, C. G. Bien, J. Bauer, H. Lassmann, The compartmentalized inflammatory response in the multiple sclerosis brain is composed of tissue-resident CD8+ T lymphocytes and B cells. *Brain* **141**, 2066–2082 (2018).
22. J. Smolders, K. M. Heutinck, N. L. Fransen, E. B. M. Remmerswaal, P. Hombrink, I. J. M. Ten Berge, R. A. W. van Lier, I. Huitinga, J. Hamann, Tissue-resident memory T cells populate the human brain. *Nat. Commun.* **9**, 4593 (2018).
23. P. B. Jahrling, C. J. Peters, Lymphocytic choriomeningitis virus. A neglected pathogen of man. *Arch. Pathol. Lab. Med.* **116**, 486–488 (1992).
24. R. Ahmed, A. Salmi, L. D. Butler, J. M. Chiller, M. B. Oldstone, Selection of genetic variants of lymphocytic choriomeningitis virus in spleens of persistently infected mice. Role in suppression of cytotoxic T lymphocyte response and viral persistence. *J. Exp. Med.* **160**, 521–540 (1984).
25. M. B. Oldstone, A suspenseful game of 'hide and seek' between virus and host. *Nat. Immunol.* **8**, 325–327 (2007).
26. G. Di Liberto, S. Pantelyushin, M. Kreutzfeldt, N. Page, S. Musardo, R. Coras, K. Steinbach, I. Vincenti, B. Klimek, T. Lingner, G. Salinas, N. Lin-Marq, O. Staszewski, M. J. Costa Jordão, I. Wagner, K. Egervari, M. Mack, C. Bellone, I. Blümcke, M. Prinz, D. D. Pinschewer, D. Merkler, Neurons under T cell attack coordinate phagocyte-mediated synaptic stripping. *Cell* **175**, 458–471.e19 (2018).
27. M. Kreutzfeldt, A. Bergthaler, M. Fernandez, W. Brück, K. Steinbach, M. Vorm, R. Coras, I. Blümcke, W. V. Bonilla, A. Fleige, R. Forman, W. Müller, B. Becher, T. Misgeld, M. Kerschensteiner, D. D. Pinschewer, D. Merkler, Neuroprotective intervention by interferon-γ blockade prevents CD8$^+$ T cell-mediated dendrite and synapse loss. *J. Exp. Med.* **210**, 2087–2103 (2013).
28. D. D. Pinschewer, M. Schedensack, A. Bergthaler, E. Horvath, W. Brück, M. Löhning, D. Merkler, T cells can mediate viral clearance from ependyma but not from brain parenchyma in a major histocompatibility class I- and perforin-independent manner. *Brain* **133**, 1054–1066 (2010).
29. D. D. Pinschewer, M. Perez, A. B. Sanchez, J. C. de la Torre, Recombinant lymphocytic choriomeningitis virus expressing vesicular stomatitis virus glycoprotein. *Proc. Natl. Acad. Sci. U.S.A.* **100**, 7895–7900 (2003).
30. E. Bettelli, M. Pagany, H. L. Weiner, C. Linington, R. A. Sobel, V. K. Kuchroo, Myelin oligodendrocyte glycoprotein-specific T cell receptor transgenic mice develop spontaneous autoimmune optic neuritis. *J. Exp. Med.* **197**, 1073–1081 (2003).
31. T. J. Schall, K. Bacon, K. J. Toy, D. V. Goeddel, Selective attraction of monocytes and T lymphocytes of the memory phenotype by cytokine RANTES. *Nature* **347**, 669–671 (1990).
32. H. Gaertner, F. Cerini, J.-M. Escola, G. Kuenzi, A. Melotti, R. Offord, I. Rossitto-Borlat, R. Nedellec, J. Salkowitz, G. Gorochov, D. Mosier, O. Hartley, Highly potent, fully recombinant anti-HIV chemokines: Reengineering a low-cost microbicide. *Proc. Natl. Acad. Sci. U.S.A.* **105**, 17706–17711 (2008).
33. I. Bartholomaus, N. Kawakami, F. Odoardi, C. Schläger, D. Miljkovic, J. W. Ellwart, W. E. F. Klinkert, C. Flügel-Koch, T. B. Issekutz, H. Wekerle, A. Flügel, Effector T cell interactions with meningeal vascular structures in nascent autoimmune CNS lesions. *Nature* **462**, 94–98 (2009).
34. P. van der Valk, S. Amor, Preactive lesions in multiple sclerosis. *Curr. Opin. Neurol.* **22**, 207–213 (2009).
35. M. P. Crawford, S. X. Yan, S. B. Ortega, R. S. Mehta, R. E. Hewitt, D. A. Price, P. Stastny, D. C. Douek, R. A. Koup, M. K. Racke, N. J. Karandikar, High prevalence of autoreactive, neuroantigen-specific CD8$^+$ T cells in multiple sclerosis revealed by novel flow cytometric assay. *Blood* **103**, 4222–4231 (2004).
36. N. A. Danke, D. M. Koelle, C. Yee, S. Beheray, W. W. Kwok, Autoreactive T cells in healthy individuals. *J. Immunol.* **172**, 5967–5972 (2004).
37. A. N. Theofilopoulos, D. H. Kono, R. Baccala, The multiple pathways to autoimmunity. *Nat. Immunol.* **18**, 716–724 (2017).
38. B. Engelhardt, P. Vajkoczy, R. O. Weller, The movers and shapers in immune privilege of the CNS. *Nat. Immunol.* **18**, 123–131 (2017).
39. Q. Ji, A. Perchellet, J. M. Goverman, Viral infection triggers central nervous system autoimmunity via activation of CD8$^+$ T cells expressing dual TCRs. *Nat. Immunol.* **11**, 628–634 (2010).
40. N. Page, B. Klimek, M. De Roo, K. Steinbach, H. Soldati, S. Lemeille, I. Wagner, M. Kreutzfeldt, G. Di Liberto, I. Vincenti, T. Lingner, G. Salinas, W. Brück, M. Simons, R. Murr, J. Kaye, D. Zehn, D. D. Pinschewer, D. Merkler, Expression of the DNA-binding factor TOX promotes the encephalitogenic potential of microbe-induced autoreactive CD8$^+$ T cells. *Immunity* **48**, 937–950.e8 (2018).
41. G. K. Binder, D. E. Griffin, Interferon-γ-mediated site-specific clearance of alphavirus from CNS neurons. *Science* **293**, 303–306 (2001).
42. J. Herz, K. R. Johnson, D. B. McGavern, Therapeutic antiviral T cells noncytopathically clear persistently infected microglia after conversion into antigen-presenting cells. *J. Exp. Med.* **212**, 1153–1169 (2015).
43. L. G. Guidotti, T. Ishikawa, M. V. Hobbs, B. Matzke, R. Schreiber, F. V. Chisari, Intracellular inactivation of the hepatitis B virus by cytotoxic T lymphocytes. *Immunity* **4**, 25–36 (1996).
44. N. S. Heaton, R. A. Langlois, D. Sachs, J. K. Lim, P. Palese, B. R. tenOever, Long-term survival of influenza virus infected club cells drives immunopathology. *J. Exp. Med.* **211**, 1707–1714 (2014).
45. J. Jo, U. Aichele, N. Kersting, R. Klein, P. Aichele, E. Bisse, A. K. Sewell, H. E. Blum, R. Bartenschlager, V. Lohmann, R. Thimme, Analysis of CD8$^+$ T-cell–mediated inhibition of hepatitis C virus replication using a novel immunological model. *Gastroenterology* **136**, 1391–1401 (2009).
46. H. Moriuchi, M. Moriuchi, A. S. Fauci, Nuclear factor-kappa B potently up-regulates the promoter activity of RANTES, a chemokine that blocks HIV infection. *J. Immunol.* **158**, 3483–3491 (1997).
47. P. Génin, M. Algarte, P. Roof, R. Lin, J. Hiscott, Regulation of RANTES chemokine gene expression requires cooperativity between NF-κB and IFN-regulatory factor transcription factors. *J. Immunol.* **164**, 5352–5361 (2000).
48. B. J. Swanson, M. Murakami, T. C. Mitchell, J. Kappler, P. Marrack, RANTES production by memory phenotype T cells is controlled by a posttranscriptional, TCR-dependent process. *Immunity* **17**, 605–615 (2002).
49. A. Marcais, M. Tomkowiak, T. Walzer, C.-A. Coupet, A. Ravel-Chapuis, J. Marvel, Maintenance of CCL5 mRNA stores by post-effector and memory CD8 T cells is dependent on transcription and is coupled to increased mRNA stability. *Eur. J. Immunol.* **36**, 2745–2754 (2006).
50. A. Song, Y.-F. Chen, K. Thamatrakoln, T. A. Storm, A. M. Krensky, RFLAT-1: A new zinc finger transcription factor that activates RANTES gene expression in T lymphocytes. *Immunity* **10**, 93–103 (1999).
51. C. Schläger, H. Körner, M. Krueger, S. Vidoli, M. Haberl, D. Mielke, E. Brylla, T. Issekutz, C. Cabañas, P. J. Nelson, T. Ziemssen, V. Rohde, I. Bechmann, D. Lodygin, F. Odoardi, A. Flügel, Effector T-cell trafficking between the leptomeninges and the cerebrospinal fluid. *Nature* **530**, 349–353 (2016).
52. K. J. Kennedy, R. M. Strieter, S. L. Kunkel, N. W. Lukacs, W. J. Karpus, Acute and relapsing experimental autoimmune encephalomyelitis are regulated by differential expression of the CC chemokines macrophage inflammatory protein-1alpha and monocyte chemotactic protein-1. *J. Neuroimmunol.* **92**, 98–108 (1998).
53. M. Matsui, J. Weaver, A. E. I. Proudfoot, J. R. Wujek, T. Wei, E. Richer, B. D. Trapp, A. Rao, R. M. Ransohoff, Treatment of experimental autoimmune encephalomyelitis with the chemokine receptor antagonist Met-RANTES. *J. Neuroimmunol.* **128**, 16–22 (2002).
54. E. H. Tran, W. A. Kuziel, T. Owens, Induction of experimental autoimmune encephalomyelitis in C57BL/6 mice deficient in either the chemokine macrophage inflammatory protein-1α or its CCR5 receptor. *Eur. J. Immunol.* **30**, 1410–1415 (2000).
55. W. G. Glass, J. K. Lim, R. Cholera, A. G. Pletnev, J.-L. Gao, P. M. Murphy, Chemokine receptor CCR5 promotes leukocyte trafficking to the brain and survival in West Nile virus infection. *J. Exp. Med.* **202**, 1087–1098 (2005).
56. B. Molon, G. Gri, M. Bettella, C. Gómez-Moutón, A. Lanzavecchia, C. Martínez-A, S. Mañes, A. Viola, T cell costimulation by chemokine receptors. *Nat. Immunol.* **6**, 465–471 (2005).
57. J. Skuljec, H. Sun, R. Pul, K. Bénardais, D. Ragancokova, D. Moharregh-Khiabani, A. Kotsiari, C. Trebst, M. Stangel, CCL5 induces a pro-inflammatory profile in microglia in vitro. *Cell. Immunol.* **270**, 164–171 (2011).
58. Z. R. Shaheen, A. Naatz, J. A. Corbett, CCR5-dependent activation of mTORC1 regulates translation of inducible NO synthase and COX-2 during Encephalomyocarditis virus infection. *J. Immunol.* **195**, 4406–4414 (2015).
59. B. S. Christmann, J. M. Moran, J. A. McGraw, R. M. Buller, J. A. Corbett, Ccr5 regulates inflammatory gene expression in response to encephalomyocarditis virus infection. *Am. J. Pathol.* **179**, 2941–2951 (2011).
60. J. W. Tyner, O. Uchida, N. Kajiwara, E. Y. Kim, A. C. Patel, M. P. O'Sullivan, M. J. Walter, R. A. Schwendener, D. N. Cook, T. M. Danoff, M. J. Holtzman, CCL5-CCR5 interaction provides antiapoptotic signals for macrophage survival during viral infection. *Nat. Med.* **11**, 1180–1187 (2005).

61. M. Zhou, L. McPherson, D. Feng, A. Song, C. Dong, S.-C. Lyu, L. Zhou, X. Shi, Y.-T. Ahn, D. Wang, C. Clayberger, A. M. Krensky, Krüppel-like transcription factor 13 regulates T lymphocyte survival in vivo. *J. Immunol.* **178**, 5496–5504 (2007).
62. C. J. A. De Groot, E. Bergers, W. Kamphorst, R. Ravid, C. H. Polman, F. Barkhof, P. van der Valk, Post-mortem MRI-guided sampling of multiple sclerosis brain lesions: Increased yield of active demyelinating and (p)reactive lesions. *Brain* **124**, 1635–1645 (2001).
63. I. V. Allen, S. McQuaid, M. Mirakhur, G. Nevin, Pathological abnormalities in the normal-appearing white matter in multiple sclerosis. *Neurol. Sci.* **22**, 141–144 (2001).
64. R. B. Banati, J. Newcombe, R. N. Gunn, A. Cagnin, F. Turkheimer, F. Heppner, G. Price, F. Wegner, G. Giovannoni, D. H. Miller, G. D. Perkin, T. Smith, A. K. Hewson, G. Bydder, G. W. Kreutzberg, T. Jones, M. L. Cuzner, R. Myers, The peripheral benzodiazepine binding site in the brain in multiple sclerosis: Quantitative in vivo imaging of microglia as a measure of disease activity. *Brain* **123** (Pt 11), 2321–2337 (2000).
65. J. van Horssen, S. Singh, S. van der Pol, M. Kipp, J. L. Lim, L. Peferoen, W. Gerritsen, E.-J. Kooi, M. E. Witte, J. J. G. Geurts, H. E. de Vries, R. Peferoen-Baert, P. J. van den Elsen, P. van der Valk, S. Amor, Clusters of activated microglia in normal-appearing white matter show signs of innate immune activation. *J. Neuroinflammation* **9**, 156 (2012).
66. N. Collins, X. Jiang, A. Zaid, B. L. Macleod, J. Li, C. O. Park, A. Haque, S. Bedoui, W. R. Heath, S. N. Mueller, T. S. Kupper, T. Gebhardt, F. R. Carbone, Skin $CD4^+$ memory T cells exhibit combined cluster-mediated retention and equilibration with the circulation. *Nat. Commun.* **7**, 11514 (2016).
67. N. Iijima, A. Iwasaki, T cell memory. A local macrophage chemokine network sustains protective tissue-resident memory CD4 T cells. *Science* **346**, 93–98 (2014).
68. Y. Natsuaki, G. Egawa, S. Nakamizo, S. Ono, S. Hanakawa, T. Okada, N. Kusuba, A. Otsuka, A. Kitoh, T. Honda, S. Nakajima, S. Tsuchiya, Y. Sugimoto, K. J. Ishii, H. Tsutsui, H. Yagita, Y. Iwakura, M. Kubo, L. g. Ng, T. Hashimoto, J. Fuentes, E. Guttman-Yassky, Y. Miyachi, K. Kabashima, Perivascular leukocyte clusters are essential for efficient activation of effector T cells in the skin. *Nat. Immunol.* **15**, 1064–1069 (2014).
69. P. Hjelmstrom, A. E. Juedes, J. Fjell, N. H. Ruddle, Cutting edge: B-cell-deficient mice develop experimental allergic encephalomyelitis with demyelination after myelin oligodendrocyte glycoprotein sensitization. *J. Immunol.* **161**, 4480–4483 (1998).
70. S. L. Hauser, E. Waubant, D. L. Arnold, T. Vollmer, J. Antel, R. J. Fox, A. Bar-Or, M. Panzara, N. Sarkar, S. Agarwal, A. Langer-Gould, C. H. Smith; HERMES Trial Group, B-cell depletion with rituximab in relapsing-remitting multiple sclerosis. *N. Engl. J. Med.* **358**, 676–688 (2008).
71. A. F. Ramlackhansingh, D. J. Brooks, R. J. Greenwood, S. K. Bose, F. E. Turkheimer, K. M. Kinnunen, S. Gentleman, R. A. Heckemann, K. Gunanayagam, G. Gelosa, D. J. Sharp, Inflammation after trauma: Microglial activation and traumatic brain injury. *Ann. Neurol.* **70**, 374–383 (2011).
72. H. Luche, O. Weber, T. Nageswara Rao, C. Blum, H. J. Fehling, Faithful activation of an extra-bright red fluorescent protein in "knock-in" Cre-reporter mice ideally suited for lineage tracing studies. *Eur. J. Immunol.* **37**, 43–53 (2007).
73. T. Buch, F. L. Heppner, C. Tertilt, T. J. A. J. Heinen, M. Kremer, F. T. Wunderlich, S. Jung, A. Waisman, A Cre-inducible diphtheria toxin receptor mediates cell lineage ablation after toxin administration. *Nat. Methods* **2**, 419–426 (2005).
74. P. Mombaerts, J. Iacomini, R. S. Johnson, K. Herrup, S. Tonegawa, V. E. Papaioannou, RAG-1-deficient mice have no mature B and T lymphocytes. *Cell* **68**, 869–877 (1992).
75. S. M. Kallert, S. Darbre, W. V. Bonilla, M. Kreutzfeldt, N. Page, P. Müller, M. Kreuzaler, M. Lu, S. Favre, F. Kreppel, M. Löhning, S. A. Luther, A. Zippelius, D. Merkler, D. D. Pinschewer, Replicating viral vector platform exploits alarmin signals for potent $CD8^+$ T cell-mediated tumour immunotherapy. *Nat. Commun.* **8**, 15327 (2017).
76. L. Flatz, A. Bergthaler, J. C. de la Torre, D. D. Pinschewer, Recovery of an arenavirus entirely from RNA polymerase I/II-driven cDNA. *Proc. Natl. Acad. Sci. U.S.A.* **103**, 4663–4668 (2006).
77. M. M. McCausland, S. Crotty, Quantitative PCR technique for detecting lymphocytic choriomeningitis virus in vivo. *J. Virol. Methods* **147**, 167–176 (2008).
78. F. Cerini, H. Gaertner, K. Madden, I. Tolstorukov, S. Brown, B. Laukens, N. Callewaert, J. C. Harner, A. M. Oommen, J. T. Harms, A. R. Sump, R. C. Sealock, D. J. Peterson, S. K. Johnson, S. B. Abramson, M. Meagher, R. Offord, O. Hartley, A scalable low-cost cGMP process for clinical grade production of the HIV inhibitor 5P12-RANTES in *Pichia pastoris*. *Protein Expr. Purif.* **119**, 1–10 (2016).
79. I. M. Stromnes, L. M. Cerretti, D. Liggitt, R. A. Harris, J. M. Goverman, Differential regulation of central nervous system autoimmunity by T_H1 and T_H17 cells. *Nat. Med.* **14**, 337–342 (2008).
80. A. Bergthaler, D. Merkler, E. Horvath, L. Bestmann, D. D. Pinschewer, Contributions of the lymphocytic choriomeningitis virus glycoprotein and polymerase to strain-specific differences in murine liver pathogenicity. *J. Gen. Virol.* **88**, 592–603 (2007).
81. M. J. Gerdes, C. J. Sevinsky, A. Sood, S. Adak, M. O. Bello, A. Bordwell, A. Can, A. Corwin, S. Dinn, R. J. Filkins, D. Hollman, V. Kamath, S. Kaanumalle, K. Kenny, M. Larsen, M. Lazare, Q. Li, C. Lowes, C. C. McCulloch, E. McDonough, M. C. Montalto, Z. Pang, J. Rittscher, A. Santamaria-Pang, B. D. Sarachan, M. L. Seel, A. Seppo, K. Shaikh, Y. Sui, J. Zhang, F. Ginty, Highly multiplexed single-cell analysis of formalin-fixed, paraffin-embedded cancer tissue. *Proc. Natl. Acad. Sci. U.S.A.* **110**, 11982–11987 (2013).
82. K. Steinbach, M. Piedavent, S. Bauer, J. T. Neumann, M. A. Friese, Neutrophils amplify autoimmune central nervous system infiltrates by maturing local APCs. *J. Immunol.* **191**, 4531–4539 (2013).

Acknowledgments: We thank the iGE3 genomics platform at the University of Geneva for help with expression profiling. **Funding:** D.M. was supported by the Swiss National Science Foundation (310030_173010) and the Swiss MS Society. O.H. was supported by the Swiss National Science Foundation (310030_163085). **Author contributions:** K.S. performed main experiments and corresponding data analysis. I.V. and K.E. participated in the histological processing and analysis of human tissue samples. I.V., N.P., B.K., and G.D.L. participated in the acquisition and analysis of flow cytometric data. M.K. developed and applied computer-assisted image analysis algorithms. I.W. and K.H. performed the histological tissue processing and staining. I.R.-B. and O.H. provided the 5P12-RANTES and helped in designing CCR5 blocking experiments. F.v.d.M. and C.S. prescreened the tissue of NAWM from human MS brains. A.M. and T.K. provided conceptional inputs and collaborated on T_{RM} phenotyping. D.D.P. provided support in virus generation. K.S. and D.M. wrote the manuscript. D.M. designed the project. **Competing interests:** D.M., N.P., and M.K. are inventors on a patent describing recombinant arenavirus vectors (patent application no. PCT/EP2015/076458, "Tri-segmented arenaviruses as vaccine vectors"). D.D.P. is an inventor on patents describing recombinant arenavirus vectors (patent application no. PCT/EP2015/076458, "Tri-segmented arenaviruses as vaccine vectors"; no. US8592205B2, "Replication-defective arenavirus vectors"; no. EP3458593A1, "Tri-segmented pichinde viruses as vaccine vectors") and a founder, consultant, and shareholder of Hookipa Pharma Inc., commercializing recombinant arenavirus vectors. O.H. is an inventor of 5P12-RANTES and a shareholder of Orion Biotechnology Switzerland, to whom the rights to the invention have been assigned. D.M., K.S., and O.H. are co-inventors on a patent application that describes methods of inhibiting cerebral inflammation. **Data and materials availability:** All data associated with this study are present in the paper or Supplementary Materials. 5P12-RANTES can be obtained from O.H. via a material transfer agreement.

Submitted 27 September 2018
Resubmitted 13 January 2019
Accepted 25 April 2019
Published 26 June 2019
10.1126/scitranslmed.aav5519

Citation: K. Steinbach, I. Vincenti, K. Egervari, M. Kreutzfeldt, F. van der Meer, N. Page, B. Klimek, I. Rossitto-Borlat, G. Di Liberto, A. Muschaweckh, I. Wagner, K. Hammad, C. Stadelmann, T. Korn, O. Hartley, D. D. Pinschewer, D. Merkler, Brain-resident memory T cells generated early in life predispose to autoimmune disease in mice. *Sci. Transl. Med.* **11**, eaav5519 (2019).